1

Synthetic AGB Evolution

M.A.T. Groenewegen
P. Marigo

1 The Role of Synthetic Evolutionary Models

Full stellar evolution calculations are computer-time-consuming, especially when they reach the AGB phase, reflecting the complexity of the inner structure of AGB stars and of the temporal evolution due to thermal pulses (see Chapter **??**). Therefore, if one is interested in distribution functions (for example, the luminosity function of AGB stars in a galaxy, or the fraction of AGB stars in a galaxy that are obscured by dust, or population synthesis in general), this is hardly achievable from calculating and integrating over a set of tens to hundreds of full stellar evolutionary models. In addition, full stellar models depend critically on a number of uncertain parameters, like mass loss, mixing length, and convective dredge-up of nucleosynthesis products. Clearly, it is computationally prohibitive to calculate a grid of stellar evolution models (including the AGB phase) sufficiently spaced in mass, and for different choices of initial metallicities, mass loss, and other parameters.

A complementary approach to *full evolutionary models* is provided by *synthetic evolutionary models*, with the aim to supply simplified descriptions of stellar evolution, or at least of the most important observable parameters, like the time-evolution of the total mass, atmospheric abundances, surface luminosity and effective temperature. The recipes and descriptions used in synthetic evolution are based on the results of full evolutionary models, and/or derived from empirical calibrations. Therefore, the physical correctness of synthetic evolution models can never be better than the full models they are based on. The main limitation of this approach is the unavoidable loss of detail in going from full models to synthetic models, which, in general, do not provide all the details on the internal structure of AGB stars.

On the positive side, the advantages of synthetic models are clear. First of all, the evolution of a star through the AGB phase is calculated more quickly. Hence, the enormous gain in computer time makes population synthesis readily feasible. Furthermore, it should be remarked that in looking at distribution functions of properties of AGB stars in external galaxies, the details—which are lost in synthetic evolution—are almost always washed away by observational error or are not resolved in the first place. Second, the influence of parameters like dredge-up, and mass loss, can be much more easily investigated. Third, predictions can be readily compared with observations, the reproduction of which—through calibration of key-model parameters—may give useful indications on related physical processes, and hence provide feedback to the developers of full models.

In this chapter we will provide a comprehensive overview of how a synthetic evolution program might look like. In fact, using the recipes provided, the reader may construct a workable synthetic evolution program of his own. Suggestions for improvements or extensions are included. Specifically, the organization of this chapter is the following. In Section 2 we give a brief overview of published AGB synthetic models, from pioneer to present works. Section 3 illustrates the necessary ingredients for developing a synthetic model for evolution of a single AGB star. As a next step, the basic information necessary to construct synthetic populations of AGB stars is given in Section 5. Finally, Section 6 is dedicated to presenting a few relevant observational constraints that synthetic models should reproduce, discussing them on the basis of recent results.

2 A Historical Overview

The first significant AGB synthetic model was developed by [50] (and references therein). They were primarily interested in the *s*-process nucleosynthesis occurring in AGB stars (see Chapter **??**). The most influential study was undoubtedly that of [87]. Some of the recipes they introduced are sometimes still referred to today, even if the paper is outdated by now. In this respect, it should be remarked that the [87] model was *uncalibrated*; i.e., the parameters of the relevant process (like mass loss and dredge-up) were not constrained to observations, but rather derived from then current theoretical indications. However, that work had the merit of outlining the structure and basic ingredients of all synthetic evolution models that came later. It also indicated the kind of analysis that can be done with synthetic models: For instance, their results were used to compare the theoretical luminosity function of carbon stars with the observed one in the LMC and to compare the predicted abundances in the ejecta of AGB stars with the observed abundances in planetary nebulae. Moreover, [87] calculated the amount and chemical compositions of matter returned to the interstellar medium, thus providing the key ingredients to Galactic chemical evolution models. Other studies from that epoch include [2] and [14].

In most cases the formulae used in these studies were based on full evolutionary AGB calculations for massive stars ($3 \lesssim M/\mathrm{M}_\odot \lesssim 8$). These results were then extrapolated to less-massive stars. This was one limitation of these early works. Other important aspects that had been neglected in almost all early studies were the metallicity dependence of the evolutionary algorithms used, the time variation of the luminosity (and other parameters) during the thermal-pulse cycle, and the fact that the first few pulses are not yet at full amplitude. Finally, the breakdown of the core mass-luminosity relation caused by the occurrence of hot bottom burning in the most massive AGB stars was not accounted for, since that was a later finding of full stellar models (i.e., [6]).

A synthetic evolution model that tried to incorporate the effects of metallicity dependence, time-variation over the thermal-pulse cycle, and the low amplitude of the first few pulses, and also made use of the full evolutionary models for low-mass AGB stars that appeared in the late 1980s (by Lattanzio, Boothroyd and Sackmann, and Hollowell; see Chapter **??**) was the model by [32]. Using this new synthetic model, the luminosity function of carbon stars in the LMC was fitted to determine the dredge-up parameters and efficiency of Reimers mass-loss law. In this sense the model was *calibrated*.

In other papers the model was extended to compare the abundances in the ejecta of AGB stars to those observed in planetary nebulae (PNe) in the LMC [33], compare period distributions of Mira stars in the LMC [34], check the influence of different mass-loss prescriptions [35], study the formation and evolution of Galactic carbon stars [38], and calculate the stellar yields that are needed in chemical evolution models [101].

A model that is largely based on that of [32], but that includes a much more detailed description of the nucleosynthesis, is the calibrated model by [66]. In that work the changes in the surface abundances caused by hot bottom burning are not calculated from simple approximations, but instead by solving a nuclear network for the outer envelope. This approach is more costly in computer time (though much less than full AGB stellar calculations), but is a correct procedure for a detailed analysis of hot bottom burning phenomenon.

Both the [32] and the [66] models were significant improvements over the models from the 1980s, yet the issue remained that the recipes were not derived from a uniformly calculated grid of full stellar models, and that not all recipes included a metallicity dependence. In this perspective, [107] calculated an extensive grid of full stellar models, from which [108] derived detailed recipes useful for synthetic AGB evolution, yet not for the possible changes in the surface abundances. Some of the prescriptions in [108] have already been included in some calculations, such as those presented by [63], and [68].

These latter works mark further improvements of synthetic AGB models. A method, based on envelope integrations, was first developed by [67] and [63] to account for the breakdown of the core mass–luminosity relation as a consequence of hot bottom burning in the most massive AGB stars ($M \gtrsim 3.5-$ -4 M$_\odot$). The second notable improvement concerns the treatment of the third dredge-up. In [68] a criterion, based on envelope integrations, was adopted to determine whether and when the third dredge-up occurs in a star of given mass and metallicity. Based on that, the carbon star luminosity functions in both Magellanic Clouds were reproduced, yielding a metallicity-dependent calibration of the dredge-up parameters.

3 The Main Ingredients of a Synthetic AGB Model

Synthetic AGB models are constructed on the basis of the results from full evolutionary calculations, which can be often "summarized" in the form of fitting analytical relations, and/or prescriptions derived from observations (e.g., mass loss, dredge-up efficiency). The approach can be purely analytical, or semianalytical when analytical prescriptions are coupled to numerical integrations of structural models (e.g., convective envelope models, "extended" envelope models including the nuclear burning shell(s)).

Synthetic models should easily predict the average evolution of the main physical quantities of an AGB star, such as the surface luminosity and effective temperature, the growth of the core mass during quiescent inter-pulse periods and its reduction when dredge-up occurs at thermal pulses (TPs), the changes in the surface chemical composition, the amount of material lost by stellar winds, and hence the final mass of the remnant.

To this end, the following sections are dedicated to presenting the main necessary ingredients, which should be considered as a "shopping list" for anyone intending to follow the evolution of a star on the AGB by means of a synthetic model. We also recommend that the reader refer to Chapter **??** for an exhaustive analysis of AGB stellar structure and evolution as predicted by full stellar models.

3.1 The Evolution Prior to the First Thermal Pulse

In synthetic AGB calculations, the evolution prior to the first TP should be taken into account, essentially to determine the physical conditions of a star at the onset of the thermally pulsing regime, namely, the core mass, the envelope mass possibly reduced by previous mass loss, the surface luminosity, and the envelope chemical composition.

3.1.1 Up to the Core Helium Ignition

Low-mass stars that experience the core helium flash ($M_{\rm i} < M_{\rm HeF} \approx 1.7$–$2.5$ M$_\odot$, depending on metallicity and model details) may lose a non negligible amount of mass on the Red Giant Branch (RGB). This can be easily estimated by directly applying the classical Reimers law [84] ($\dot{M}$ =

$4 \times 10^{-13} \eta\, L_* R_* / M_*\ \mathrm{M}_\odot\,\mathrm{yr}^{-1}$, where the stellar values are in solar units) for mass loss to the RGB evolutionary tracks of some stellar library (e.g., [21, 30, 80, 92]). In the standard procedure, the efficiency parameter η in the Reimers prescription should be calibrated (usually $\eta \approx 0.35$–0.40) in order to reproduce the observed morphology of horizontal branches in galactic globular clusters (see [86]).

Predictions of the surface chemical changes produced by the *first dredge-up*, occurring at the base of the RGB, can be taken as well from full stellar models, as a function of the stellar mass and chemical composition. Tables are nowadays available for sufficiently dense grids of M and Z (e.g., [30]), so that simple interpolations in the two variables can be made.

3.1.2 The Early-AGB (E-AGB)

Similarly to the RGB, the evolution along the E-AGB and the related mass loss by stellar winds can be easily derived from available sets of full stellar models—usually calculated at constant mass—to which one should then apply some mass-loss prescription. The procedure is quite simple, so that analytical fitting relations describing the evolution of the stellar parameters on the E-AGB are not given here. An analytical description of the E-AGB can be found in [108].

The expected changes in the chemical composition of the envelope due to the *second dredge-up*, occurring at the base of the E-AGB for stars with $M_\mathrm{i} \gtrsim 3.5\ \mathrm{M}_\odot$, can also be obtained from available stellar libraries.

3.2 The Thermally Pulsing (TP) AGB Phase: Some Definitions

Let us first define some quantities that are used throughout the rest of this chapter.

A *thermal pulse cycle* (TPC) is the time interval from a local maximum of helium burning, through quiescent hydrogen burning, up to the next TP.

The *core* is defined as the part of a star inside the location where the local hydrogen content reaches half the photospheric value. Since the H-burning shell is extremely narrow (both in radius and relative mass units), this essentially coincides with all other definitions of the core mass in the literature. The *core growth* ΔM_c is defined as $\int \max\{\frac{\mathrm{d}M_\mathrm{c}}{\mathrm{d}\tau}, 0\}\mathrm{d}\tau$. Usually, $\Delta M_\mathrm{c} = M_\mathrm{c}(\tau) - M_{\mathrm{c},0}$, where $M_{\mathrm{c},0}$ is the core mass at the first TP.

The *first TP* is the one in which the maximum (integrated) luminosity produced by He-burning exceeds the maximum H-burning luminosity prior to this for the first time. Before the first TP there may be *prepulses*.

We refer to *asymptotic phase* or *full-amplitude regime* when the global quantities of the TP-AGB evolution have reached their asymptotic behavior, usually after a few (pre-)pulses.

Table 1. The coefficients of Equation 1.

Z	p_1	p_2	p_3	p_4	p_5	p_6	p_7
0.02	0.0294	1.478	0.550	0.0634	0.572	3.193	0.260
0.0001	0.0213	2.589	0.592	0.0324	0.790	2.867	0.260

3.3 The Initial Conditions at the First TP

The quantities that govern the physical condition of a star at the beginning of its TP-AGB phase are the total mass M, the core mass $M_{\rm c}$, the surface luminosity L, the effective temperature $T_{\rm eff}$, and the chemical composition of the envelope.

The core mass at the first thermal pulse, $M_{\rm c,0}$, is an important quantity, since it fixes a lower limit to the remnant mass, and therefore it is closely linked to the initial–final mass relation (see Section 6.1).

We report from [108] the following equations:

$$M_{\rm c,0}(M_{\rm i}) = \left(-p_1(M_{\rm i}-p_2)^2+p_3\right) f + (p_4 M_{\rm i}+p_5)\,(1-f) \qquad (1)$$

where

$$f(M_{\rm i}) = \left(1+{\rm e}^{\frac{M_{\rm i}-p_6}{p_7}}\right)^{-1},$$

which are fitting relations to the results of full stellar calculations. The parameters p_1 to p_7 can be found in Table 1, and can be interpolated linearly in $\log Z$. The luminosity at the first TP is found by inserting the core mass at the first TP into the core mass–luminosity relation presented in Section 3.4.5.

It should be remarked that the fitting relations quoted above are derived from classical models; i.e., the convective boundaries are determined via the Schwarzschild criterion. Stellar models adopting convective overshoot would predict a similar trend for $M_{\rm c,0}(M_{\rm i})$, except that at given stellar mass the core mass is larger than in classical models (e.g., [30, 92]).

3.4 The Luminosity Evolution on the TP-AGB

In the following we briefly recall the main features of the luminosity evolution during a pulse cycle, which is depicted in Figure 1. This latter has been obtained by adopting the analytical relations presented by [108], which one should refer to for all the details (see also Section 3.4.5).

3.4.1 The Core Mass–Luminosity Relation (CMLR)

On the basis of stellar evolution calculations, [76] first discovered the existence of a simple relationship between the core mass $M_{\rm c}$ of a TP-AGB star and its quiescent interflash luminosity (part of the lightcurve around $L_{\rm A}$ in Figure 1). He derived the fitting formula in the range $0.57\ {\rm M}_\odot < M_{\rm c} < 1.39\ {\rm M}_\odot$:

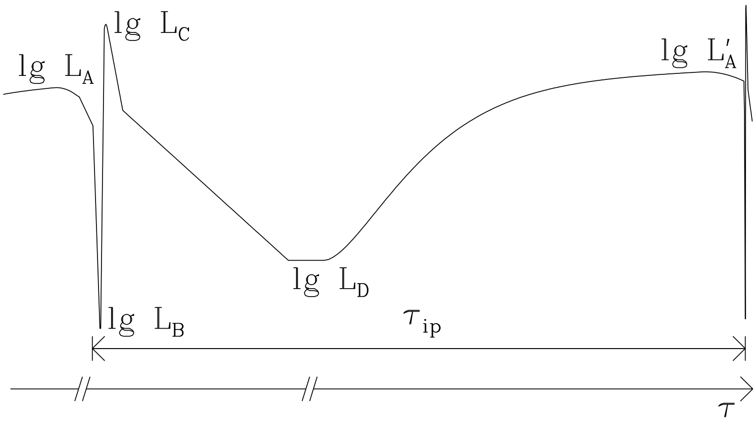

Fig. 1. Typical evolution of the surface luminosity during a thermal pulse cycle. The time axis has been stretched around the first TP shown. From [108].

$$L = 59250(M_{\rm c} - 0.522), \tag{2}$$

where masses and luminosities are in solar units.

Over the years, continuous upgrading of the input physics and detailed calculations of the AGB phase over wider ranges of stellar masses and chemical compositions resulted into a flourishing of several $M_{\rm c} - L$ relationships ([9, 41, 46, 50, 59, 108, 120]). Many of them are displayed in Figure 2.

From the most recent analysis it turns out that the CMLR contains a non negligible dependence upon the surface chemical composition; i.e., for a given core mass the luminosity is higher at increasing metal and helium contents (hence higher mean molecular weight). For instance, for core masses in the range 0.5 $M_{\odot} < M_{\rm c} < 0.66$ $M_{\odot}$, [9] derived

$$L = 238000\mu^3 (Z_{\rm CNO})^{0.04} (M_{\rm c}^2 - 0.0305 M_{\rm c} - 0.1802), \tag{3}$$

where $\mu = 4/(5X + 3 - Z)$ is the mean molecular weight under the assumption of a fully ionized gas, and $Z_{\rm CNO}$ is the fractional surface abundance (by mass) of the CNO elements. It follows that at given core mass, stars of solar composition ($Z = 0.02$, $\mu \approx 0.62$) are $\approx 25\%$ more luminous than metal-poor stars ($Z = 0.001$, $\mu \approx 0.598$).

The existence of the CMLR can be explained from first principles, under specific structural conditions that make the thermal evolution of the core be essentially decoupled from that of the outer envelope. The reader can find transparent demonstrations of this in [54, 76, 82, 99].

It should be emphasized that the structure of a TP-AGB star fulfills the conditions necessary for a CMLR to exist only in particular stages of the evolution, i.e., during the quiescent part of the pulse cycle (when the H-burning shell supplies most of the stellar energy), provided that the full-amplitude

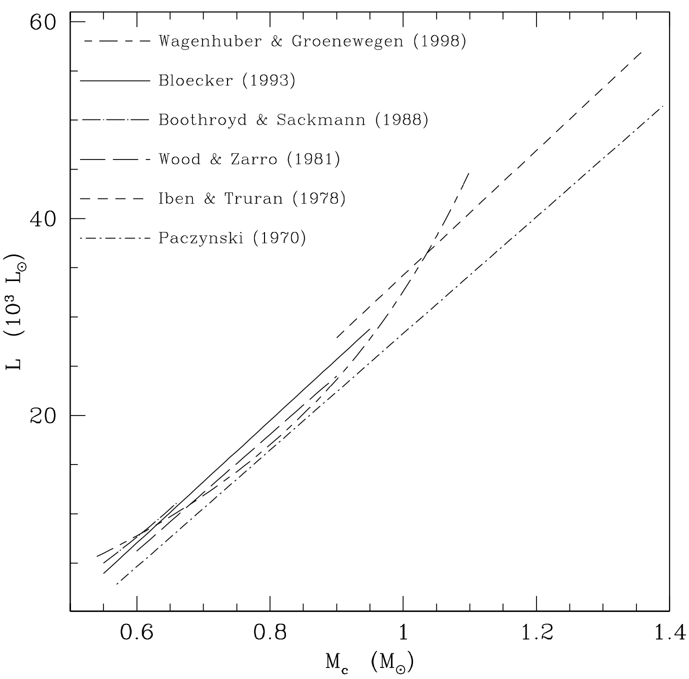

Fig. 2. CMLRs from various authors, each plotted in the range of $M_{\rm c}$ considered to obtain the analytical fit to the model results. Where a composition dependence is present, the solar case is considered, i.e., $(Z = 0.02, Y = 0.28)$. The relation by Iben & Truran [50] refers to a 7 M$_\odot$ model.

regime has been attained, and hot bottom burning (HBB, see later in this section) is not operating.

Out of these specific phases, the luminosity evolution of a TP-AGB star does not follow the CMLR listed above. The main deviations, which should be included in synthetic calculations, are briefly recalled and discussed in the following.

3.4.2 The Subluminous Prepulses

The onset of thermal pulses usually takes place at lower luminosities than predicted by the standard CMLR for the same core mass. Moreover, the initial evolution of the quiescent interpulse luminosity as a function of $M_{\rm c}$ approaches the asymptotic regime of full amplitude with a steeper slope than that of the CMLR (e.g., [9]). Recently, [44] have reported that the occurrence of the third dredge-up already at the first thermal pulses may alter the approach toward the full amplitude regime, possibly preventing the settlement onto the CMLR (but see also [70]).

3.4.3 Flash-Driven Luminosity Variations: Peaks and Dips

The occurrence of a TP may cause significant variations of the surface luminosity as long as the thermal instability is removed and quiescent H-burning recovered. The most significant features following a TP are shown in Figure 1, namely, (i) the rapid dip (fast luminosity drop indicated by $L_{\rm B}$), (ii) the post-thermal-pulse luminosity peak (rapid rise of light curve up to the maximum denoted by $L_{\rm C}$), and (iii) the slow dip (subluminous part of the pulse cycle labeled $L_{\rm D}$). These features have amplitudes and durations that depend on stellar parameters, mainly envelope mass and metallicity (see [8] for a detailed analysis).

It should be remarked that the subluminous slow dip is that of the greatest significance, since it may produce observable and testable effects, especially during the evolution of the lowest-mass stars. These can spend as much as 20%–30% of the interpulse period at a luminosity a factor of two lower than predicted by the CMLR for the same core mass. As a consequence, the slow dip is found to importantly affect the faint wing of the carbon star luminosity function (see Section 6.2), and may explain the observed mixture of carbon- and oxygen-rich stars at the same luminosities (e.g., [69]).

3.4.4 Over-Luminosity Produced by Hot Bottom Burning (HBB)

In the most luminous and massive TP-AGB stars ($M_{\rm i}\gtrsim$ 3.5 M$_{\odot}$) the base of the convective stellar envelope can deepen into high-temperature regions ($T > 20 - 40 \times 10^6$ K) so that H-burning via the CNO cycle can occur. This process is called hot bottom burning (HBB) or envelope burning. The most notable signature of its occurrence is the breakdown of the CMLR toward higher luminosities, as first pointed out by [6], and confirmed by subsequent studies (e.g., [7, 12, 20, 61, 106]).

The violation of the CMLR produced by HBB should be included in modern AGB synthetic calculations, provided that the results of full AGB models can be reproduced. To this end, substantial efforts have been recently performed by [63, 67, 108]. In the former work a solution method, based on envelope integrations, has been developed in order to account for the production of nuclear energy at the base of the convective envelope; the latter study presents analytical fitting relations derived from complete calculations of AGB models with HBB.

Both works successfully reproduce the expected luminosity evolution of a massive TP-AGB star with HBB, as a function of model parameters (i.e., mass-loss rates, mixing length parameter), and stellar parameters (i.e., current envelope mass, metallicity). An example of synthetic calculations (from [63]) is illustrated in Figure 3, showing the luminosity evolution of a ($5\,{\rm M}_{\odot}, Z =$

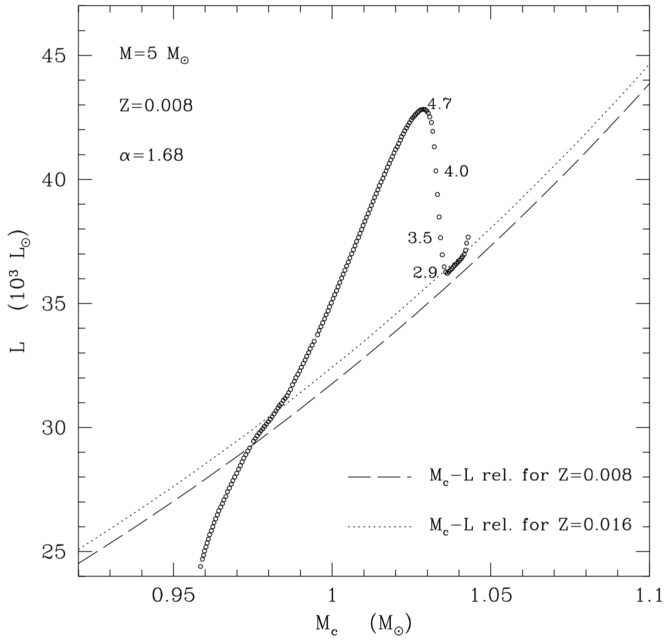

Fig. 3. Luminosity evolution of a $5.0\,\mathrm{M}_\odot$, $Z = 0.008$ star experiencing HBB. The open circles correspond to the maximum quiescent luminosity before each thermal pulse. The numbers along the curve indicate the current stellar mass in solar units. The dashed and dotted lines represent the reference CMLR relation [108] for $Z = 0.008$ and $Z = 0.016$, respectively. From [63].

0.008) model as a function of the core mass. Mass loss is included according to the [106] formalism.

We can notice that HBB develops since the first subluminous interpulse periods, so that when thermal pulses attain the full-amplitude regime the star does not settle on the CMLR (dashed line), but quickly reaches higher and higher luminosities, with a brightening rate much greater than expected from the slope of the standard relation. The luminosity increases as long as the stellar envelope is massive enough to maintain high temperatures at its bottom. The luminosity maximum and subsequent decline are determined by the onset of the superwind, when the star starts to rapidly lose mass at significant rates (i.e., $\dot{M} \approx 10^{-5}$ to $10^{-4}\,\mathrm{M}_\odot\,\mathrm{yr}^{-1}$). Due to the drastic reduction of the stellar envelope mass, HBB weakens and eventually extinguishes. As a consequence, the star approaches again the CMLR, where it lies till the end of the evolution.

It is worth remarking that owing to the dependence of the CMLR on the chemical composition, the star finally recovers a CMLR consistent with an increased stellar envelope metallicity due to the combined effect of the third dredge-up and HBB (see Figure 3).

3.4.5 Useful Analytical Relations

Analytical formulas describing secular light curves of TP-AGB stars, based on extensive grids of evolutionary calculations for stars with initial masses in the range 0.8 $M_\odot \leq M_\mathrm{i} \leq 7$ $M_\odot$, and metallicities $Z = 0.0001$, $Z = 0.008$, and $Z = 0.02$, have recently been presented by [108]. The maximum luminosity during quiescent H-burning is given as the sum of different terms:

$$\begin{aligned} L = & (18160 + 3980 \log \tfrac{Z}{0.02})(M_\mathrm{c} - 0.4468) && (4a)\\ & + [\ 10^{2.705+1.649 M_\mathrm{c}} && (4b)\\ & \quad \times 10^{0.0237(\alpha-1.447) M_{\mathrm{c},0}^2 M_\mathrm{env}^2 (1-e^{-\Delta M_\mathrm{c}/0.01})}\ ] && (4c)\\ & -10^{3.529-(M_{\mathrm{c},0}-0.4468)\Delta M_\mathrm{c}/0.01} && (4d) \end{aligned}$$

The first term (4a) represents the classical linear $M_\mathrm{c} - L$ relation, giving the quiescent luminosity for stars already in the full-amplitude regime, with core masses in the range 0.6 $M_\odot \lesssim M_\mathrm{c} \lesssim 0.95$ $M_\odot$. The second term (4b) provides a correction, becoming significant for high values of the core mass $M_\mathrm{c} >$ 0.95 $M_\odot$. The third term (4c) accounts for the extra luminosity produced by HBB, as a function of the stellar envelope mass M_env. A dependence on the mixing-length parameter, α, is included to reproduce the strength of HBB on the basis of calculations carried out by [107] with $\alpha = 1.5$, and other authors, namely, [7] with $\alpha = 2.1$, [20] with $\alpha = 2.75$. Finally, the fourth term (4d) gives a negative correction to the luminosity in order to mimic the subluminous and steep evolution typical of the first pulses.

We recall that in [108] the reader can find many other useful analytical relations, e.g., describing the flash-driven variations already mentioned in Section 3.4.3.

3.5 The Time Evolution on the TP-AGB

The time evolution of a TP-AGB star is essentially determined by the outward advance of the H-burning shell, which lasts for most of the interpulse period, τ_ip. After this, the next thermal pulse occurs, possibly followed by a dredge-up event that reduces the core mass, and a new pulsecycle starts.

3.5.1 The Rate of Core Growth During the Interpulse Period

The equation that describes the rate of core growth reads

$$\frac{dM_c}{dt} = \frac{q}{X} L i H, \qquad (5)$$

where X is the hydrogen abundance (in mass fraction) in the stellar envelope, L_{H} is the luminosity produced by the H-burning shell, and q is the mass burnt per unit of energy released. Following [108], it turns out that q is slightly metallicity dependent due to the contribution from the pp-cycle for low Z. The calculations with a nuclear network yield the mean value $q = [(1.02 \pm 0.04) + 0.017(Z/0.02)]10^{-11}\ \mathrm{M}_{\odot}\,\mathrm{L}_{\odot}^{-1}\,\mathrm{yr}^{-1}$.

The luminosity produced by H-burning (L_{H}) that enters Equation 5 is lower than the total luminosity, since gravitational energy release due to the core shrinking and the flow of burnt envelope material down to the core, together with relic He-burning, additionally contribute during quiescent H-burning. According to [108], the relative contribution from H-burning to the inter-pulse surface luminosity as given by their equation (1.4) (part of the light curve labeled L_{A} in Figure 1) is

$$\lg(LiH/L) = -0.012 - 10^{-1.25-113\Delta M_{\mathrm{c}}} - 0.0016 M_{\mathrm{env}}. \tag{6}$$

This equation has been derived from complete AGB models without HBB, i.e., with the term (4c) set to unity.

3.5.2 The Core Mass–Interpulse Period Relation

The time-scale characteristic of a thermal pulse, τ_{ip}, which is the time interval between two subsequent pulses, is a decreasing function of the core mass as first pointed out by [77],

$$\log \tau_{\mathrm{ip}} = 4.5\,(1.678 - M_{\mathrm{c}}), \tag{7}$$

and subsequently confirmed by complete AGB calculations (e.g., [10, 120]). In the work of [10] a strong dependence on composition was found: At the same core mass, τ_{ip} for the low-metallicity case (e.g., $Z = 0.001$) is found to be nearly twice as long as in the high-metallicity case (e.g., $Z = 0.02$).

The recent relation presented by [108] is

$$\begin{aligned} \log \tau_{\mathrm{ip}} = {} & (-3.628 + 0.1337\ \log \tfrac{Z}{0.02})\ (M_{\mathrm{c}} - 1.9454) && \text{(8a)} \\ & -10^{-2.080-0.353\ \log \frac{Z}{0.02} + 0.200(M_{\mathrm{env}}+\alpha-1.5)} && \text{(8b)} \\ & -10^{-0.626-70.30\ (M_{\mathrm{c},0}-\log \frac{Z}{0.02})\ \Delta M_{\mathrm{c}}}. && \text{(8c)} \end{aligned}$$

Three components can be distinguished: The term (8a) expresses τ_{ip} as a decreasing exponential function of M_{c} with some dependence on the metallicity; the term (8b) gives a negative correction to include the effect of hot bottom burning in somewhat reducing the interpulse period; and term (8c) reproduces the initial increase of τ_{ip} starting from values that are shorter by almost a factor of two compared to those derived from the asymptotic relation for the same core mass.

3.6 The Effective Temperature

The effective temperature, $T_{\rm eff}$, can be determined in two possible ways, either (1) using semiempirical calibrations, or (2) with the aid of stellar envelope integrations.

Empirical prescriptions can be derived, for instance, by coupling observations of AGB variables with measured periods and light curves (e.g., Miras) to pulsation model atmospheres, in which the effective temperature is made to vary until good spectral and light-amplitude fits are obtained (e.g., [4, 13]). This allows one to get a relation between the bolometric luminosity and effective temperature, including some dependence on the stellar mass and metallicity (e.g., [118]).

The purely theoretical approach, based on stellar envelope models, requires that four boundary conditions be specified in order to integrate the four equations of stellar structure for L_r, T_r, P_r (or ρ_r), and r as a function of the Lagrangian mass coordinate M_r. Let us denote by M, L, P, R, $T_{\rm eff}$ the photospheric values, and assume that M, $M_{\rm c}$, and the chemical composition of the homogeneous convective envelope are given.

Two outer boundary conditions are immediately available: The effective stellar surface radius is determined by the Stefan-Boltzmann law, and the photospheric pressure can be derived as $P = P(L, M, T_{\rm eff})$ from the integration of a stellar atmosphere model; see Chapter **??**.

The third condition can be derived, for instance, considering that the transition to the core is very well defined, due to the extreme steepness of the structural gradients in a very thin region below the base of the convective envelope. In other words, we can safely assume that the Lagrangian mass coordinate of the base of the envelope coincides with that of the core.

These three conditions are sufficient to solve the stellar envelope structure up to the photosphere (hence to determine $T_{\rm eff}$) if no energy source is present inside the envelope, i.e., when HBB is not operating. In this circumstance the integration of the equation of thermal balance can be skipped, just setting $L_r = L$, i.e., the luminosity is constant throughout the envelope. We recall that during quiescent H-burning L is determined by the CMLR (see Section 3.4.1).

Differently, in massive AGB stars with HBB, not only does the surface luminosity depend on $M_{\rm c}$, but it is also affected by the physical properties of the stellar envelope itself (e.g., envelope mass, temperature, and density stratification) as well as by model prescriptions (e.g., mixing-length parameter, overshooting). All these factors actually affect the efficiency of nuclear rates in the deepest layers of the envelope. The fourth boundary condition is then needed. Possible boundary conditions can be figured out with the aid of complete calculations of the AGB phase. For instance, one could adopt the *core mass–core radius relation* for AGB stars to determine the radial coordinate below which a mass equal to $M_{\rm c}$ should be contained. Another alternative is to constrain the local energy flux at the base of the convective envelope to be the sum of the energy contributions from the gravitational contraction of the core, He-burning shell, and radiative layers of the H-burning shell. Physical and technical details on envelope integrations are extensively described in [63, 66, 87, 90, 108, 120].

Stellar envelope integrations in synthetic AGB models are also useful for quickly exploring the sensitivity of the results to different input prescriptions, such as the mixing-length parameter α, nuclear reaction rates, and gas opacities. For instance, [65] has recently investigated the remarkable effects produced by molecular opacities if properly coupled to the actual carbon and oxygen surface abundance, hence C/O ratio. This point is discussed in Section 6.3.

3.7 Mass Loss by Stellar Winds

Mass loss by stellar winds plays a crucial role in the evolution of an AGB star, since it not only determines the final mass at the end of the AGB and hence the final luminosity, but it also affects its internal structure and nucleosynthesis. Many mass-loss prescriptions for the AGB phase have been suggested over the years, based on both theoretical arguments (e.g., [1, 7, 13, 24]) and/or (semi-) empirical calibrations (e.g., [106]), which have proved to give a better description of mass-loss rates than the classical Reimers law [84].

This latter was originally designed to account for mass loss along the RGB (see Section 3.1.1). The adoption of the Reimers law does not account for the highest mass loss rates observed in stars close to the tip of the AGB ($\dot{M} \approx 10^{-5} - 10^{-4} \mathrm{M}_{\odot}\ \mathrm{yr}^{-1}$), being also inadequate to explain the ejection of planetary nebulae at the observed luminosities. A sudden transition to the so-called *superwind* regime should then be invoked to reconcile predictions to observations [87]. High mass-loss rates can be obtained with Reimers-like prescriptions only by adopting quite large values of the efficiency parameter (e.g., $\eta = 5$ as in [32]). A natural development of the super wind is instead allowed by more recent prescriptions for mass loss (e.g., [24, 106]) that consider the combined role of radiation pressure, stellar pulsation, and dust formation in driving mass loss on the AGB. Moreover, it turns out that mass loss depends on metallicity, roughly as $\approx Z^{0.5}$, as suggested from both theoretical ([57, 103]) and observational ([37]) evidence. In addition, since mass loss seems to correlate with luminosity, and the luminosity varies over the TP-cycle, mass loss variations on a time scale of 10^4 years are implied (see Section 6.6).

The effect of different mass-loss prescriptions on the predicted initial–final mass relation and its dependence on the chemical composition will be discussed in Section 6.1, on the basis of synthetic AGB calculations.

3.8 Surface Chemical Changes During the TP-AGB

We will illustrate here the basic schemes for describing the main processes that may change the surface chemical composition of an AGB star, namely, the third dredge-up and hot bottom burning.

3.8.1 The Third Dredge-Up

A synthetic treatment of the third dredge-up requires three basic inputs:

- the minimum core mass $M_{\rm c}^{\rm min}$ for dredge-up to occur;
- the efficiency λ;
- the chemical composition of the material being dredged up.

A TP-AGB star can experience the third dredge-up if its core mass has grown over a critical value $M_{\rm c}^{\rm min}$, as indicated by theoretical analysis of thermal pulses (e.g., [11, 49, 60, 117]).

The quantity λ expresses the dredge-up efficiency, since it measures the extent of the inward penetration of the convective envelope. It is defined as the fraction of the core mass increment, $\Delta M_{\rm c}$, during the preceding inter-pulse period that is dredged up to the surface by envelope convection:

$$\lambda = \frac{\Delta M_{\rm dredge}}{\Delta M_{\rm c}}, \tag{9}$$

where $\Delta M_{\rm dredge}$ is the mass of the dredged-up material.

Finally, the chemical composition of the dredged-up material coincides with that of the convective intershell that develops during a thermal pulse, mainly containing ^{4}He and the nuclear products of alpha-captures (C and O).

Once the three parameters are specified, the new surface abundance of a given element $Y_i^{\rm new}$ soon after a dredge-up event can be calculated,

$$Y_i^{\rm new} = \frac{Y_i^{\rm old} M_{\rm env} + Y_i^{\rm cs} \Delta M_{\rm dredge}}{M_{\rm env} + \Delta M_{\rm dredge}}, \tag{10}$$

where $Y_i^{\rm old}$ and $M_{\rm env}$ are the stellar envelope abundance and mass before the dredge-up, respectively; $Y_i^{\rm cs}$ is the elemental abundance in the convective intershell, hence in the dredged-up material.

In principle, the aforementioned parameters in synthetic AGB models could be specified following the predictions of full AGB calculations. From doing so in past works (e.g., [87]) a clear discrepancy between observations and predictions emerged: Theory predicted too few faint (single) carbon stars, an aspect of the so-called *carbon star mystery* first pointed out by [47].

In this context, [32], [66], and [68] have moved from another perspective: The dredge-up parameters are adopted as free parameters to be calibrated on the observed luminosity functions of carbon stars in the Magellanic Clouds. The discrepancy could be removed assuming, on average, lower $M_{\rm c}^{\rm min}$ and larger λ than found in full evolutionary calculations.

In recent years the detailed treatment of the third dredge-up has been improved, leading, in some cases, to an earlier occurrence and a greater efficiency than in previous calculations (e.g., [43, 44, 94]).

The real values of $M_{\rm c}^{\rm min}$ are still a matter of debate, since this quantity heavily depends on the delicate interplay between model prescriptions (e.g.,

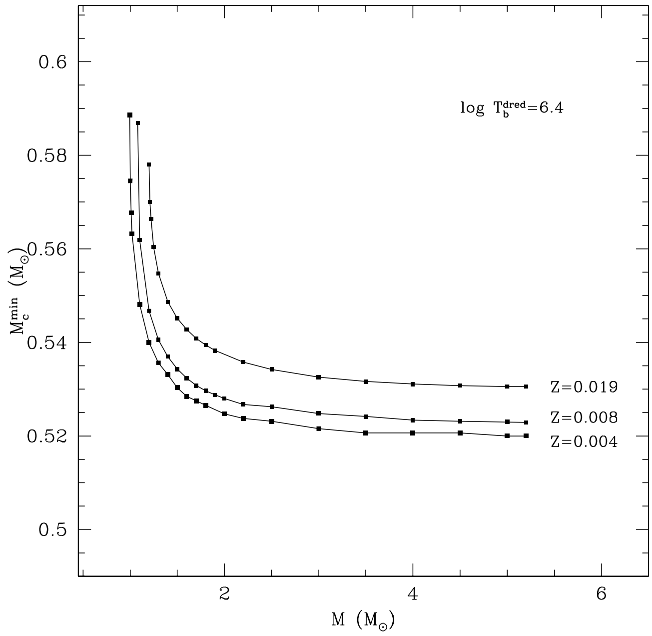

Fig. 4. Predicted behavior of the minimum core mass for the third dredge-up, $M_{\rm c}^{\rm min}$, as a function of the actual stellar mass, for three values of the initial metallicity, and assuming the specified value for the minimum temperature at the base of the convective envelope ($T_{\rm b}^{\rm dred}$). From [68].

opacities, nuclear reaction rates, mixing-length parameter, mass loss, time and mass resolution) and intrinsic properties of the star (e.g., chemical composition, stellar envelope mass, strength of the pulse). Nevertheless, a certain trend can be extracted from full stellar models; i.e., the onset of the third dredge-up is favored (i.e., $M_{\rm c}^{\rm min}$ is lower) at higher stellar mass M, lower metallicity Z, and greater efficiency of envelope convection (e.g., obtained by increasing the mixing-length parameter).

The estimation of $M_{\rm c}^{\rm min}$ in synthetic models has been recently improved by [68] following the scheme proposed by [117]. The usual criterion based on a constant $M_{\rm c}^{\rm min}$ parameter is replaced by one on the minimum temperature at the base of the convective stellar envelope, $T_{\rm b}^{\rm dred}$, at the stage of the post-thermal-pulse luminosity maximum. Envelope integrations allow one then to determine $M_{\rm c}^{\rm min}$ as a function of stellar mass, metallicity, and pulse strength, thus implying whether and when dredge-up first occurs. Predictions for $M_{\rm c}^{\rm min}$ are shown in Figure 4, as a function of stellar mass and metallicity. It turns out that the onset of the third dredge-up is favored in stars with lower metallicity and larger mass. The $T_{\rm b}^{\rm dred}$ criterion can also predict the possible shutdown of the process, e.g., in the last stages of the AGB evolution when the envelope mass is drastically reduced and the minimum base temperature is no longer attained.

The question of the real values of λ is also troublesome, since it is crucially affected by the treatment (both physical and numerical) of the instability of matter against convection (see, e.g., [27, 72]). It should be remarked that the difficulty of earlier complete AGB models in finding significant dredge-up (e.g., [28, 49, 117]), particularly in faint low-mass stars, still affects many recent calculations (e.g., [106, 107]). However, recent analysis would indicate that such a problem can be overcome, either on the basis of technical improvements [94], or by allowing for deep extra mixing beyond the formal convective boundaries ([44, 72]). However, these latter AGB calculations still need to be extended to the lowest stellar masses and over a larger range of metallicities, and then tested through a full comparison with observations of carbon stars.

Conversely, a limitation still affecting AGB synthetic calculations is that λ is often assumed a constant parameter, regardless of current mass and metallicity. On the basis of recent complete AGB calculations with deep extra mixing, [72] suggests an analytical fitting formula

$$\lambda = 7 \times (M_{\rm c} - 0.571) \tag{11}$$

expressing the efficiency of the third dredge-up as a function of the core mass. The correctness of this law has still to be tested through systematic synthetic calculations.

The chemical composition of the dredge-up material is also affected by model details. According to full calculations of the third dredge-up and related nucleosynthesis, after the first peculiar pulses the intershell approaches a typical chemical composition, in which the distribution of the elements seems to be crucially dependent on the treatment of the convective boundaries, with [$X(^4{\rm He}) \approx 0.76$; $X(^{12}{\rm C}) \approx 0.22$; $X(^{16}{\rm O}) \approx 0.02$] according to classical models based on the Schwarzschild criterion (e.g., [10]); and [$X(^4{\rm He}) \approx 0.25$; $X(^{12}{\rm C}) \approx 0.50$; $X(^{16}{\rm O}) \approx 0.25$] following the recent results by [44] based on the adoption of a deep overshooting.

For all the reasons mentioned, the treatment of the third dredge-up in synthetic models is preferably a parametric one; that is, the parameters are not assumed a priori, but calibrated on observations (i.e., carbon star luminosity functions). This important application will be discussed in detail in Section 6.2, on the basis of recent AGB synthetic calculations.

3.8.2 Nucleosynthesis During HBB

The changes in surface abundances (e.g., H, He, C, N, O) caused by HBB during the interpulse evolution of the most massive AGB stars should be taken into account in synthetic AGB models. This can be done either (i) by directly solving a specified nuclear network (see, for instance, the works by

[67, 87, 90]), or (ii) by adopting a parametric scheme like that suggested by [32], to which the reader is referred for a description.

In case (i), static stellar envelope integrations can be used to determine, at each time step, the temperature and density stratification across the envelope. Then, the changes in elemental abundances can be obtained by directly solving the system of differential equations, of the kind

$$\frac{dY_i}{dt} = -[ij]\ Y_i Y_j + [rs]\ Y_r Y_s, \qquad i = 1, ..., N_{\rm el}, \tag{12}$$

where $N_{\rm el}$ is the number of elemental species involved; $Y_i = X_i/A_i$, X_i, and A_i denote the abundance by number (mole g^{-1}), the abundance by mass, and the atomic mass of the elemental species i, respectively. On the right-hand side of equation (12), $[ij]$ stands for the rate of the generic reaction that converts the element i into another nucleus because of the interaction with the element j, whereas $[rs]$ is the rate of the generic reaction transforming nuclei s and r into the element i.

The system of Equations (12) can be solved locally, i.e., in each layer of the stellar envelope. Finally, the new chemical composition of the envelope can be determined by mass-averaging the new local abundances in each layer throughout the envelope; i.e., it is equivalent to assume that convective currents completely homogenize the envelope composition.

3.8.3 Some Exemplifying Calculations

As mentioned in Section 3.8.1, the main processes that may alter the surface abundances of TP-AGB stars are (i) the third dredge-up, and (ii) H-burning via the CNO cycle (HBB) in the hottest stellar envelope layers of the most massive AGB stars. The former essentially determines the enrichment in primary ^{12}C, ^{16}O, ^{4}He, and s-process elements. The latter mainly leads to the increase of ^{13}C abundance at the expense of that of ^{12}C and, if reactions of the CNO cycle proceed further on, so as to allow an efficient synthesis of ^{14}N.

Figures 5 and 6 exemplify the typical evolution of the CNO surface abundances during the TP-AGB phase caused by (1) sole third dredge-up as in the $2.5\,\mathrm{M}_\odot$ model; (2) third dredge-up *and* HBB as in the $5\,\mathrm{M}_\odot$ model.

Case of Sole Third Dredge-Up

As far as the $2.5\,\mathrm{M}_\odot$ model (left-hand side panel) is concerned, the following points are worthy of notice: The transition to carbon star (as soon as $\mathrm{C/O} > 1$) after the first few thermal pulses, the increase of the $^{12}\mathrm{C}/^{13}\mathrm{C}$ ratio, the modest increase of the ^{16}O abundance, and the concomitant small decrease of the N/O ratio. Of course, these results are highly dependent on the adopted chemical distribution of the intershell, and the efficiency of envelope penetration, expressed by the parameter $\lambda = 0.5$, which has been calibrated

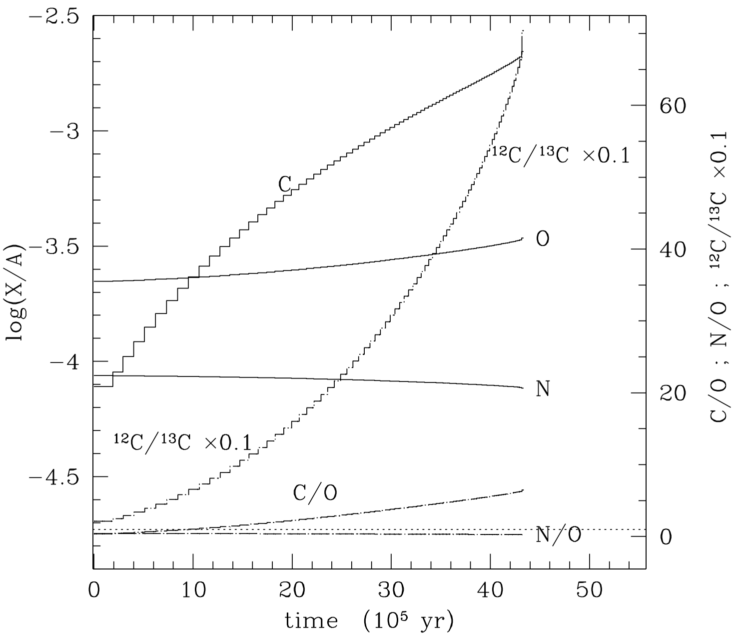

Fig. 5. Evolution of CNO surface abundances (by number, mole gr^{-1}) and ratios from the first thermal pulse until the complete ejection of the stellar envelope for $Z = 0.008$ TP-AGB model with initial mass of $2.5\,\mathrm{M}_\odot$. The efficiency parameter for the third dredge-up is assumed to be $\lambda = 0.5$; the mixing-length parameter is $\alpha = 2.0$. Based on synthetic calculations by [63].

in this case on the luminosity function of carbon stars in the LMC (cf. Section 6.2).

Case of Third Dredge-Up and HBB

The saw-like trend of the C and ^{12}C/^{13}C curves for the $5\,\mathrm{M}_\odot$ model (right-hand side panel) is caused by the combined effect of the convective dredge-up events at each thermal pulse, clearly visible in the sudden spikes, and HBB during the subsequent interflash period, which quickly converts newly dredged-up ^{12}C first into ^{13}C and then into ^{14}N.

The initial increase of both C abundance and ^{12}C/^{13}C ratio, due to the sole effect of the third dredge-up, is followed by a rapid drop as soon as HBB has become efficient enough to convert carbon isotopes into nitrogen via the first reactions of the CN cycle. *The* ^{12}C/^{13}C *ratio attains and keeps its equilibrium*

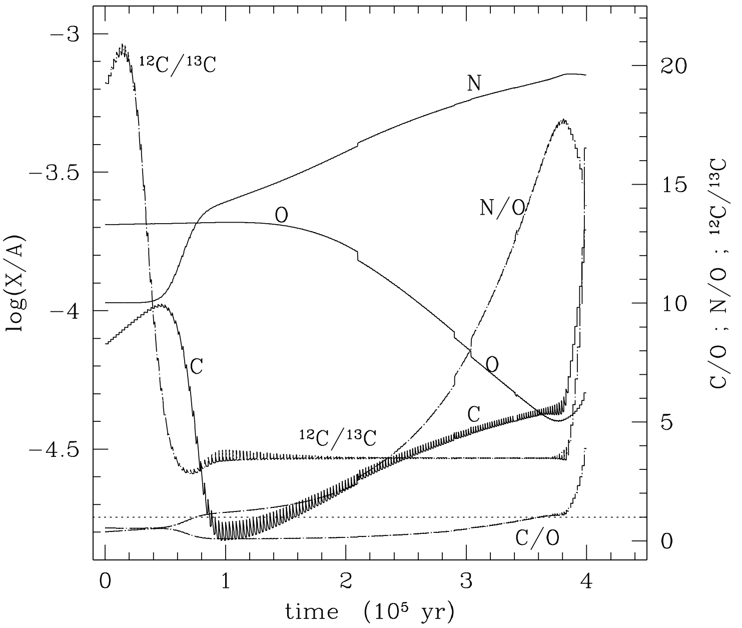

Fig. 6. The same as in Figure 5 but for a $Z = 0.008$ TP-AGB model with initial mass of $5.0\,\mathrm{M}_{\odot}$.

value of $\approx$ *3.4*, until the last stages of the evolution, when the drastic reduction of the stellar envelope mass causes a sudden extinction of nuclear reactions.

Note that for most of the TP-AGB lifetime the star is expected to be oxygen-rich; i.e., the C/O ratio is below unity. In other words, *HBB may delay or even prevent the formation of carbon stars at high luminosities*. In this case, the transition to a carbon star eventually happens when HBB weakens and ^{12}C enrichment due to convective dredge-up becomes dominant. Observationally, this would correspond to the so-called obscured carbon stars [105] being optically invisible because of the dense dusty circumstellar envelope ejected during the superwind regime (cf. [26]).

The oxygen abundance remains practically unchanged for nearly half the TP-AGB lifetime. This holds as long as the base temperature, $T_{\rm b}$, of the convective envelope has not become high enough to activate the ON cycle (^{16}O has the longest nuclear lifetime against proton captures). When this happens, for $T_{\rm b} \gtrsim 80 \times 10^6$ K, ^{16}O is efficiently destroyed.

The main product of the CNO bicycle is ^{14}N, as illustrated by the rising of the nitrogen curve. The decrease of oxygen and the rise of nitrogen both concur to significantly increase the N/O ratio up to a factor of ≈ 40. In general, HBB is expected to be an important source of nitrogen, a prediction that may be relevant for the interpretation of the overabundance of this element measured in the atmospheres of some giant stars and PNe, as well as of its observed distribution in galaxies of different metallicities.

3.8.4 Secondary and Primary Synthesis of CNO Nuclei

During the TP-AGB evolution of stars that undergo HBB, at each dredge-up event some primary ^{12}C and ^{16}O nuclei (produced by α-capture reactions) are injected into the stellar envelope, where they can partake in the CNO cycle for the conversion of hydrogen into helium. As a consequence, the surface distribution of the CNO nuclei consists of two components:

- a *secondary component* produced by nuclear reactions involving only seed metals originally present in the star at the epoch of its formation;
- a *primary component* synthesized by a chain of nuclear burnings beginning from H and He and hence independent of the original metal content.

Hence, the surface abundance (by number) Y_i of the element i belonging to the CNO group at an instant t, can be expressed as $Y_i = Y_i^{\mathrm{S}} + Y_i^{\mathrm{P}}$, where Y_i^{S} and Y_i^{P} are the secondary and primary fractions, respectively.

In Figure 7 the evolution of secondary and primary ^{12}C, ^{13}C, ^{14}N, ^{15}N, ^{16}O, ^{17}O, and ^{18}O surface abundances is plotted as a function of time for a $4.5\,\mathrm{M}_\odot$ TP-AGB star with $Z = 0.004$. It can be noticed that in this case, for all CNO nuclei the primary component (which is initially equal to zero) of the surface abundance grows such that it overcomes the secondary one.

4 Stellar Yields

Low- and intermediate-mass stars play an important role in galactic chemical evolution, thanks to the ejection into the interstellar medium of material containing newly synthesized nuclear products. These stars contribute to the chemical enrichment of the ISM essentially during the RGB and AGB phases, both characterized by the occurrence of both mass loss and events of surface chemical pollution. The most relevant contribution concerns ^{4}He, ^{12}C, and ^{14}N, but also the s-process elements (see [98] and references therein).

In the following, first we briefly recall the basic equations for the calculation of the stellar yields, and then show the predictions for the main CNO isotopes, based on recent synthetic AGB models.

4.1 Derivation of the Wind Contributions

According to the classical definition by [95], the *stellar yield*, $p_k(m)$, of a given chemical element k is the mass fraction of a star with initial mass m

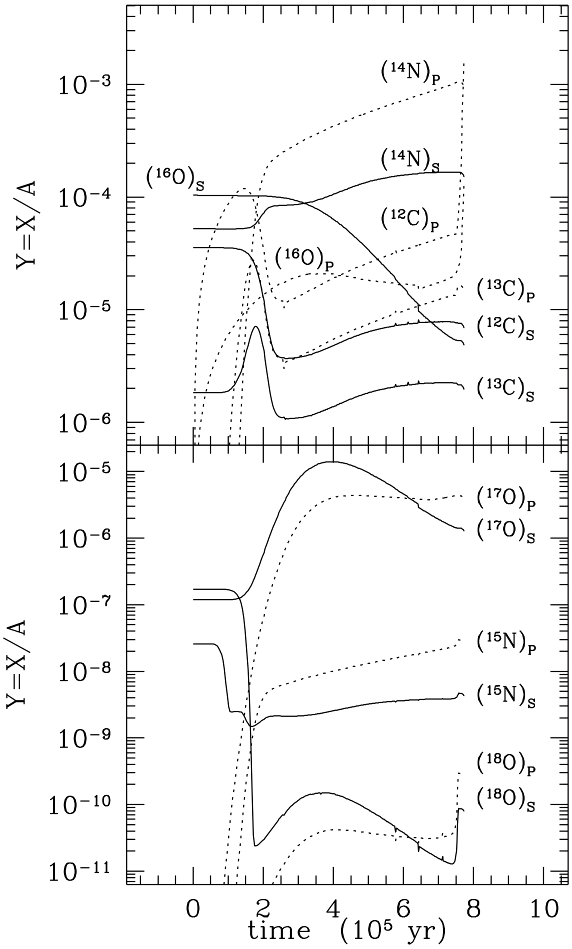

Fig. 7. Secondary and primary surface abundances (mole gr^{-1}) of CNO isotopes for a ($4.5\,\mathrm{M}_\odot$, $Z = 0.004$) model evolving on the TP-AGB phase. The adopted mixing length parameter is $\alpha = 2.0$, and the third dredge-up efficiency is $\lambda = 0.65$. Taken from synthetic AGB models by [63].

that is converted into the element k and returned to the ISM during its entire lifetime, $\tau(m)$. It follows that the quantity

$$M_{\mathrm{y}}(k) = m\,p_k(m) \tag{13}$$

gives the mass of the ejected matter in the form of the newly synthesized element k, which can be calculated by

$$M_{\mathrm{y}}(k) = \int_0^{\tau(m)} [X_k(t) - X_k^0], \dot{M}(t)dt \tag{14}$$

where $\dot{M}(t)$ represents the mass-loss rate at the current time t, and $X_k(t)$, X_k^0 denote the current and initial surface abundances of the element k, respectively. The calculation of total wind contributions should account for any

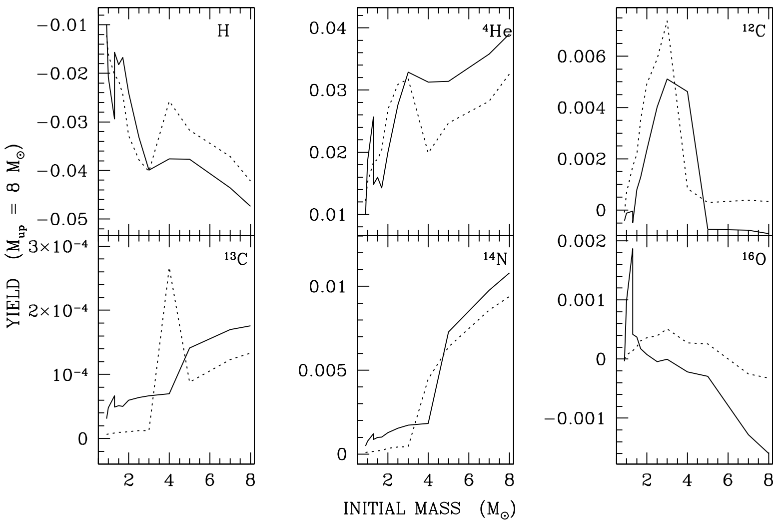

Fig. 8. Stellar yields, $p_k(m)$, from low- and intermediate mass stars, taken from calculations by [101] with $M_{\rm up} = 8{\rm M}_\odot$, for initial metallicities $Z = 0.02$ (solid line) and $Z = 0.004$ (dotted line).

possible change of elemental species caused, for instance, by the first, second, third dredge-up, and HBB. According to Equation 14, *negative* $p_{\rm k}$ correspond to those elemental species that are prevalently *destroyed* and diluted in the stellar envelope, so that their abundances in the ejected material are lower with respect to the main sequence values. In contrast, *positive* $p_{\rm k}$ correspond to those elements that are prevalently *produced*, so that a net enrichment of their abundances in the ejecta is predicted.

4.2 Yields as a Function of $M_{\rm i}$ and Z

Figures 8 and 9 show the fractional yields $p_{\rm k}$ as a function of the initial stellar mass and two choices of the metallicity, taken from two sets with different values of the upper mass limit $M_{\rm up}$ (i.e., [64, 101]). Despite some differences, in both works the predicted yield of a given elemental species displays a similar trend with the initial mass and metallicity.

- **H and ^{4}He**: The net yields of these elements have mirror-like behaviors, corresponding to a destruction of H during the synthesis of ^{4}He. The peak in ^{4}He production at around 2–3 M$_\odot$ (depending on metallicity) is mainly due to the fact that stars in this mass range have the longest TP-AGB lifetimes, so that they suffer the largest number of dredge-up events. The increase of ^{4}He yields toward higher masses, $M_{\rm i} \geq 3.5\,{\rm M}_\odot$, is favored by the occurrence of both dredge-up and HBB, depending on both the efficiency

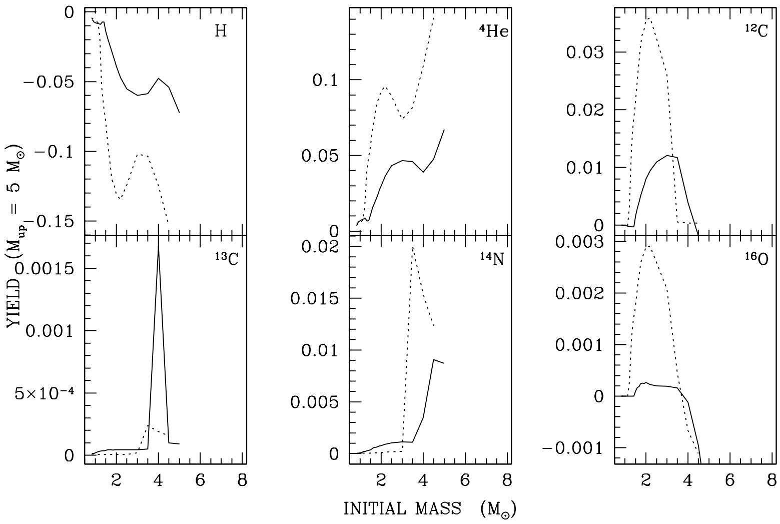

Fig. 9. The same as in Figure 8, but data taken from [64], with $M_{\rm up} = 5\,{\rm M}_\odot$.

and duration of the processes. At decreasing metallicity, the synthesis of new ^{4}He is favored by the larger efficiency of HBB in the models by [64], whereas the shorter TP-AGB lifetimes produce the opposite effect in the results of [101].

- ^{12}**C**: The net positive yield increases with the initial mass, with a production peak at about 2–3 M$_\odot$, which corresponds to stars experiencing the largest number of dredge-up episodes on the TP-AGB. The subsequent decline at increasing stellar mass is first determined by the decrease of the TP-AGB lifetimes, and then by the prevailing effect of HBB, so that the ^{12}C yield from the most massive stars finally becomes negative. It is worth noticing that both in the [64] and [101] results the peak of ^{12}C production moves toward lower initial masses for decreasing metallicities, reflecting the longer TP-AGB duration and greater efficiency of HBB.
- ^{13}**C**: The positive ^{13}C yields result mainly from the first dredge-up in lower-mass stars, and mild HBB in the most massive AGB models as long as the creation of ^{13}C via the reaction ^{12}C$(p,\gamma)^{13}$C prevails over destruction via the reaction ^{13}C$(p,\gamma)^{14}$N. The results also depend on the interplay between the efficiency of HBB and stellar winds. A suitable tuning between the strength of HBB and mass loss can occasionally create favorable conditions for the synthesis of ^{13}C, giving a peak of the related yields around $4\,{\rm M}_\odot$ for $Z = 0.02$ in [101], and for $Z = 0.004$ in [64]. In these cases, the efficiency of CNO-cycle reactions allows the synthesis of ^{13}C for a long time before the drastic reduction of the envelope mass causes the extinction of nuclear burning.

- ^{14}**N**: The surface abundance of ^{14}N can increase as a consequence of the second dredge-up and HBB, the latter process being the major cause of the synthesis of this element in intermediate-mass stars. It turns out that at decreasing metallicities, nitrogen production by HBB is favored by the larger nuclear reaction rates and/or longer TP-AGB lifetimes. It is worth remarking that low- and intermediate-mass stars play an important role in the galactic nucleosynthesis of nitrogen. As already mentioned in Section 3.8.4, AGB stars with HBB ($M_{\rm i} \gtrsim 3.5\,{\rm M}_{\odot}$) provide a source of primary ^{14}N, which is synthesized as newly dredged-up ^{12}C is injected into the CNO cycle. This primary contribution could be relevant in explaining the observed lack of a correlation between the [N/Fe] and [Fe/H] ratios in systems of very low metallicities, where a large scatter is observed (see the review by [71]).
- ^{16}**O**: The third dredge-up may determine a positive net yield of this element for stars with $0.8\,{\rm M}_{\odot} \lesssim M_{\rm i} \lesssim 3.5\,{\rm M}_{\odot}$, whereas at larger masses HBB produces an opposite effect. The results are found to significantly depend on metallicity. At decreasing metallicities larger positive yields of oxygen are expected, reflecting the longer duration of the TP-AGB (and hence the greater number of dredge-up episodes). As expected, the trend of ^{16}O is similar to that of ^{12}C.

5 From One Star to Population Synthesis

With the recipes described in Section 3, the TP-AGB evolution of a single star with given initial mass and metallicity can be calculated. The basic structure of a synthetic TP-AGB model for single-star evolution is outlined in Section 5.1.

Then, if one is interested in reproducing and interpreting the observed distribution functions of specific properties of the cool giants belonging to a stellar cluster or galaxy, the next step is to model a population of AGB stars. To this end, it is necessary to integrate the properties of single stars over the range of relevant masses. A suitable population synthesis approach is described in Section 5.2.

5.1 A Simple Scheme to Calculate the Synthetic Evolution of a Single TP-AGB Star

1. Set up the initial conditions at the first thermal pulse (M, $M_{\rm c}$, L, $T_{\rm eff}$, envelope chemical composition), and specify the basic model parameters (e.g., mass-loss law, dredge-up efficiency λ).
2. Set up counters that keep track of the number of thermal pulses and the phase within the current TPC.
3. The main loop on the sequence of TPCs starts.
4. The secondary loop on the current TPC starts.

5. Test the criterion for the third dredge-up to take place (e.g., $M_c > M_c^{min}$): If satisfied, the core mass is reduced and the stellar envelope mass is increased by the amount $\lambda \Delta M_c$, and the envelope chemical abundances are changed according to Equation 10.
6. Calculate the interpulse period, e.g., via the M_c-τ_{ip} relation described in Section 3.5.2. The inner loop on the quiescent interpulse period τ_{ip} starts.
7. Determine the time step. There are three relevant time scales: the growth of the core, mass loss from the star, and the changes in the luminosity over the TPC. No general formula can be given, and several recipes can be tried out. For example, one would like to resolve each TPC with N steps, which would lead to one estimate of the time step. Another estimate could come from the condition that mass loss cannot reduce the total mass by more than a certain amount. The time step to be chosen is then the smallest of those considered. Then, for each time step Δt:
   a) Calculate the increment of the core mass, ΔM_c, according to Equation 5.
   b) Derive the variation of the luminosity as a function of the TPC phase according to Section 3.4.
   c) Estimate the possible changes in the envelope chemical composition due to HBB nucleosynthesis for the more massive models, as outlined in Section 3.8.2.
   d) Single out the variation of the effective temperature as described in Section 3.6, via either analytical recipes or stellar envelope integrations.
   e) Calculate the amount of ejected mass, $\Delta M_{ej} = \dot{M} \Delta t$, by stellar winds, so that the current stellar mass becomes $M = M - \Delta M_{ej}$.
   f) Update all variables at the current time $t = t + \Delta t$.
   g) Test the criterion for determining the AGB termination: If satisfied go to step 8.
   h) Go back to step 7 if the current TPC has not ended yet. Otherwise, a new thermal pulse occurs, hence update the corresponding number pulse, and go back to step 4.
8. End of the main loop started at step 3, corresponding to the termination of the AGB evolution. The ending conditions are reached either (i) when the core mass has grown to the Chandrasekhar limit of about $1.4\,M_\odot$, which would imply explosive carbon ignition (this might happen for massive stars with low mass-loss rates), or (ii) when the stellar envelope mass has been reduced to some prescribed small value, of order $0.01\,M_\odot$ or less.

5.2 A Simple Scheme to Construct a Synthetic AGB Population

Stars that are presently on the AGB must have been born an appropriate time ago, so that their mass-distribution function $N(M)$ (in number of stars per unit mass interval) may be written as

$$N(M)dM \propto \int_0^{t_{\rm AGB}(M,Z)} \phi(M)\ \psi(T_G - \tau(M,Z) - x)\, dx,$$

where ϕ (in ${\rm M_\odot}^{-1}$) is the initial mass function (IMF, usually written in the form of a power law $\propto M^{-\alpha}$), ψ (in ${\rm M_\odot\,yr^{-1}}$) is the star formation rate (SFR), $t_{\rm AGB}$ is the lifetime of a star on the AGB, $T_{\rm G}$ is the age of the system, and $\tau(M)$ is the pre-AGB lifetime of a star with mass M.

Realizing that $t_{\rm AGB} \ll \tau$ for all masses leads to

$$N(M)dM \ \propto \ \phi(M)\psi(T_{\rm G} - \tau(M,Z))t_{\rm AGB}(M,Z) \tag{15}$$

in the range $M_{\rm low} < M < M_{\rm up}$, where $M_{\rm low}$ and $M_{\rm up}$ are the lower and upper mass limits, respectively, of stars that can potentially evolve through the AGB. These are constrained, respectively, by the age of the galaxy [i.e., $\tau(M_{\rm low}) \approx T_{\rm G}$), and the maximum mass for a star to develop a degenerate C-O core, with typical values of about $0.9\,{\rm M_\odot}$ and $8\,{\rm M_\odot}$ (lowered to 5–6 ${\rm M_\odot}$ in the case of models with convective overshoot). More restricted mass intervals could be specified according to particular ages of interest.

The other relevant ingredient is the age–metallicity relation. Low-mass stars, born a long time ago, have main-sequence metallicities that are lower than those of stars born today. Examples of age–metallicity and star-formation rate relations for our Galaxy can be found in [16, 88, 89] or [100]; for the Magellanic Clouds in [45] and [78]. In order to use such a relation one needs as well a relation between τ and mass (and metallicity). Such a relation can be found in [48], which unfortunately is independent of metallicity, or, by interpolation, in any published set of evolutionary tracks.

Finally, one needs to know $t_{\rm AGB}$. Because this depends on the evolution of the stars in the population under study, its value can be determined only iteratively. Since in Equation 15 only the relative ages are of importance, the dependence of the distribution of stars over mass does not depend very much on $t_{\rm AGB}$ (see Appendix B in [32]). One viable approach would be to start with (1) a constant value for $t_{\rm AGB}$, (2) run the model and adjust the parameters to fit the observations, (3) determine $t_{\rm AGB}(M)$ for that set of parameters, and (4) use this new estimate, and repeat the calculations until differences in the results fall below a predetermined tolerance.

Here we outline the logical path of steps to develop a synthetic AGB population model, based on the Monte Carlo simulation method. It is worth recalling that as an alternative, the AGB could be populated analytically, using the basic equations of population synthesis (see, e.g., [66]).

1. Read in, or set up: The initial mass function, star formation rate, age–metallicity relation, (initial mass)–(pre-AGB-lifetime) relation. Specify the mass (hence age) interval of interest.
2. Randomly draw a mass within the specified interval, according to the probability function that a star of a given mass is on the AGB at present (see Equation 15). Determine the corresponding main sequence metallicity. This may require an iteration scheme, since the pre-AGB lifetime

depends on mass but also on metallicity. One solution would be to choose an initial metallicity, then calculate the pre-AGB lifetime for that mass and metallicity, and subsequently use the age–metallicity relation to get a better estimate for the metallicity.

3. Run the routine described in Section 5.1 to predict the synthetic TP-AGB evolution of the specified single star. At each time step, update the distribution functions (of, e.g., luminosity, effective temperature, mass loss, final mass, chemical properties) you are keeping track of.
4. The procedure ends when a predetermined number of stars is randomly picked up and the distribution functions can be built.

6 Observational Constraints

6.1 The Initial-Final Mass Relation (IFMR)

The final fate of an AGB star is determined by the competition between the growth of the core mass and the mass loss by stellar winds. If the core mass is allowed to grow up to the Chandrasekhar limit ($M_{\rm c} \approx 1.4\,{\rm M}_{\odot}$), then explosive carbon ignition would occur (type I-1/2 supernova; see [49]). Conversely, if this circumstance is prevented by the the complete shedding of the stellar envelope, then the end-product of the AGB evolution is a C-O white dwarf (WD).

Establishing the relation between the final mass, $M_{\rm f}$, left at the end of the AGB, and the initial mass, $M_{\rm i}$, of the progenitor star is of paramount importance for various aspects related to both stellar evolution and the history of the host galaxy. The age of a coeval stellar system can in principle be derived once the mass of the detected WDs is empirically estimated. In particular, the initial–final mass relation (IFMR) for low- and intermediate-mass stars is an important tool for investigating the history of the Galaxy, e.g., to estimate the age of the local disk ([48, 116]). Moreover, the IFMR provides information on the total amount of mass that each star loses in the course of its entire evolution and hence on the evolution of the mass budget of stellar populations and galaxies [85]. Finally, assessing the upper mass limit for WD progenitors is a crucial aspect, since it affects the expected rate of type II supernovae events with important implications for the star formation history, the chemical enrichment of the interstellar medium, and the birth rate of neutron stars [112].

In Figure 10, a few empirical IFMRs for the solar neighborhood are displayed (top left-hand side panel). Note that the most recent studies (e.g., [42, 53, 56, 83, 111]) have notably changed the shape of the relation with respect to the earlier determination by [109], as recently discussed by [110] and [111]. The IFMR presented by [42], for instance, presents a flat slope up to Hyades location ($M_{\rm i} \approx 3\,{\rm M}_{\odot}$, $M_{\rm f} \approx 0.7\,{\rm M}_{\odot}$), followed by a steeper rise, and a final flattening toward higher initial masses ($M_{\rm i} > 4\,{\rm M}_{\odot}$). Another important

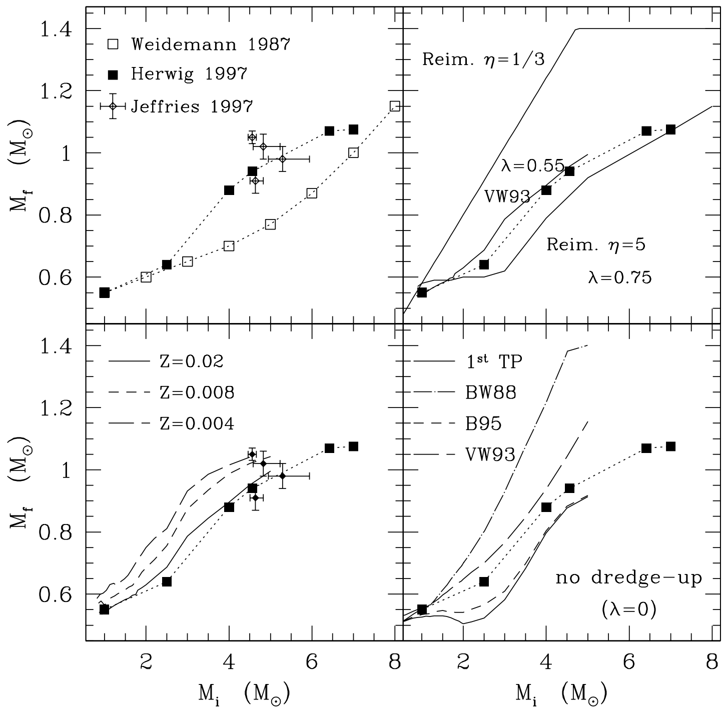

Fig. 10. Initial–final mass relation for low- and intermediate-mass stars. Top left-hand side panel: Empty and filled squares correspond to the semiempirical relation for the solar neighborhood by [109] and [42], respectively. Data from [53] are shown by points with error bars. Top right-hand side panel: Theoretical predictions for models with solar metallicity and various mass-loss prescriptions, i.e., according to [49] with the Reimers law ($\eta = \frac{1}{3}$); according to [64] with mass loss from [106]; [101] with the Reimers law ($\eta = 5$). For the two latter models, the adopted dredge-up efficiency parameter is specified. Bottom left-hand side panel: Theoretical predictions for various metallicities [64]. Bottom right-hand side panel: Theoretical predictions by [29] for models with solar metallicity, according to various mass-loss laws, i.e., [7, 13, 106]. In these calculations no dredge-up is allowed during the TP-AGB phase. The core mass at the first thermal pulse is also shown (solid line).

point concerns the expected value for $M_{\rm WDpro}$, i.e., the maximum initial mass for the WD progenitors, which is still a matter of debate. For the same open cluster NGC 2516 [56] and [83] derive $M_{\rm WDpro} \approx 8\,{\rm M}_{\odot}$, whereas [53] estimates $M_{\rm WDpro} \approx 5$–$6\,{\rm M}_{\odot}$. The former value of the limiting mass would be consistent with classical evolutionary models, the latter supporting stellar models with overshooting.

As far as the theoretical predictions of the IFMR are concerned, the following remarks should be made. Thanks to the computational agility of synthetic AGB models, these are suitable tool for a systematic investigation of the IFMR through its dependence on various parameters (e.g., mass loss prescription, dredge-up law, luminosity evolution, metallicity).

Past synthetic AGB models (e.g., [49, 87]) have predicted IFMRs in clear disagreement with the observed calibrations, i.e., a sizable excess of WDs more massive than $0.7\,\mathrm{M}_{\odot}$, with the most massive stars building C-O cores up to the Chandrasekhar value of $1.4\,\mathrm{M}_{\odot}$. We can notice the quick divergency at increasing mass that characterizes the relation predicted by [49] (top right-hand side panel in Figure 10). Actually, the WDs belonging to the youngest open clusters in the solar neighborhood have estimated masses not larger than about $1.1\,\mathrm{M}_{\odot}$ ([53, 56, 109]).

The main reason for such a discrepancy in earlier theoretical studies resides in the adoption of unsuitable mass-loss prescriptions for the AGB, i.e., the straightforward application of the Reimers law [84] originally calibrated on RGB stars. In this respect we recall that as already noticed by [87], the Reimers formula (with $\eta = \frac{1}{3}$ to 1) is not able to predict the "superwind" mass loss rates ($\dot{M} \approx 10^{-5}$ to $10^{-4}\,\mathrm{M}_{\odot}\,\mathrm{yr}^{-1}$) required to account for the typical masses (and expansion velocities) of observed PNe. Since then, high mass-loss rates, consistent with superwind values, have actually been measured in the brightest AGB stars (e.g., OH/IR and Mira variables) of the Galaxy (cf. [55]) and Magellanic Clouds (cf. [105, 119]); see Chapter **??**.

In more recent years, several prescriptions have been proposed to specifically describe mass loss during the AGB (e.g., [7, 13, 24, 106]). All these studies rely (either from theoretical arguments and/or empirical evidence) on the fact that radiation pressure, pulsation, and dust should play an essential role in driving mass loss on the AGB; see Chapters **??** and **??**. The reader can refer to [35] and [29] for an exhaustive comparison of the mostly used laws, based on various observational constraints in addition to the observed IFMR (e.g., the carbon star luminosity function, the number ratio of carbon-rich to oxygen-rich stars, chemical abundances in PNe, integrated V-K colors in LMC clusters).

The relevant point to be stressed here is that, with these new formalisms adopted in synthetic AGB models, the expected IFMRs are in better agreement with observations, if compared to those predicted by the Reimers law. This can be seen in Figure 10, which displays several theoretical IFMRs.

From these calculations we can derive a first important result. At least for not extremely low metallicities (i.e., $Z > 0.001$), even the most massive AGB stars are likely to lose all the residual stellar envelope before their C-O cores reach the Chandrasekhar mass. This would prevent the occurrence of the so-called type I-1/2 SNe, first introduced by [49].

Another relevant point is the dependence of the IFMR on the metallicity of the stellar generation. Stars with the same initial masses build up final C-O cores of larger masses at decreasing metallicity (see the bottom left-hand side panel of Figure 10). In a simple picture, this result can be explained by two concurring effects expected at lower metallicities in stars of given initial masses: (i) Stars already enter the TP-AGB phase with larger C-O cores left at the end of the He-burning phase; (ii) the location of the Hayashi lines in the HR diagram is characterized by higher effective temperatures, thus yielding lower mass-loss rates.

In addition to the mentioned points, there are additional factors that may, however, affect the resulting IFMR, namely, (iii) the dredge-up process taking place at thermal pulses, and (iv) the overluminosity produced by HBB in the most massive AGB stars.

Every time a dredge-up event occurs, it is assumed to instantaneously reduce the core mass by the quantity $\Delta M_{\rm dredge} = \lambda \Delta M_{\rm c}$, where $\Delta M_{\rm c}$ is the increment of the core mass over the previous interpulse period (see Equation 9). Following recent full calculations of thermal pulses [44] it turns out that λ could be even larger than unity, so that in this case the core mass is effectively reduced. The impact of this new scenario on the resulting IFMR deserves, however, further calculations as well as observational tests. Another effect produced by the third dredge-up on the IFMR is indirectly related to the changes in the surface chemical composition. The enrichment in carbon (and oxygen) may affect the relevant molecular absorption and dust features in the stellar atmosphere, and hence the efficiency of mass loss.

As far as the occurrence of HBB is concerned, it turns out that the steeper luminosity increase with the core mass (if compared with the classical CMLR) anticipates the transition to the superwind regime, concurring to produce remnants with lower masses. This circumstance could help to explain the flattening of the empirical IFMR toward larger initial masses. Finally, we should remark that the IFMR at larger initial masses may be influenced by HBB nucleosynthesis, since the changes in the stellar envelope abundances (mainly the increase of nitrogen) may affect the effective temperature, and hence the mass-loss rate.

The sensitivity of the IFMR to the changes in the surface chemical composition of stars with different initial masses (and chemical evolution) is an important aspect, which, however, still deserves future theoretical analysis.

6.2 The Carbon Star Luminosity Function

The observed carbon star luminosity function (CSLF) represents a fundamental constraint to AGB models, since a sole observable contains a number of implications, concerning both the evolution of single stars (e.g., evolutionary rates, mass-loss efficiency, lifetimes, initial–final mass relation, dredge-up law), and integrated properties of the host systems (e.g., star formation history, age–metallicity relation).

The need for a systematic analysis of all these factors makes synthetic AGB models the suitable tool to investigate the CSLF. Essentially, two theoretical approaches can be used to derive the predicted number, $N_{\rm k}$, of carbon stars in each $k^{\rm th}$ luminosity bin, namely:

1. analytical method (cf. [68]);

2. Monte Carlo simulation method (cf. [32]).

Clearly, both methods should produce the same results for large numbers of carbon stars.

In the former scheme, denoting by $N_k(M_i)$ the number of carbon stars with a progenitor mass M_i and a present luminosity within the $k^{\rm th}$ bin, the number N_k of carbon stars populating the $k^{\rm th}$ bin is simply given by integration of $N_k(M_i)$ over all masses M_i:

$$
\begin{aligned}
N_k &= \int_{M_{\rm i}^{\rm min}}^{M_{\rm i}^{\rm max}} N_k(M_{\rm i}) dM_{\rm i} \\
&\propto \int_{M_{\rm i}^{\rm min}}^{M_{\rm i}^{\rm max}} \psi(M_{\rm i})\ \phi[T_{\rm G} - \tau(M_{\rm i})]\ \Delta\tau_k(M_{\rm i})\ dM_{\rm i},
\end{aligned}
\tag{16}
$$

where $\psi(M_{\rm i})$ is the IMF, $T_{\rm G}$ is the age of the galaxy, $\tau(M_{\rm i})$ is the stellar lifetime, $\phi[T_{\rm G} - \tau(M_{\rm i})]$ corresponds to the star formation rate evaluated at the birth epoch of the stars of initial mass $M_{\rm i}$, and $\Delta\tau_k(M_{\rm i})$ is the time each carbon star of mass $M_{\rm i}$ spends in the $k^{\rm th}$ luminosity interval.

The latter scheme is a probabilistic one in which, given a selected sample of AGB stars, the corresponding initial masses are randomly assigned according to the distribution function in Equation 15. Once the present status (i.e., whether it is a carbon star or not, and its luminosity) of every sample star is determined, the luminosity distribution can be derived by summing up the number of carbon stars in each luminosity bin. Both methods require that the minimum ($M_{\rm min}$) and maximum ($M_{\rm max}$) initial masses for a star to become a carbon star be specified.

These methods have been successfully employed in recent synthetic AGB models (i.e., [32, 68]) aimed at reproducing the observed CSLFs in the Magellanic Clouds, via the calibration of the dredge-up parameters ($M_{\rm c}^{\rm min}$ and λ; see Section 3.8.1). Both works conclude that the third dredge-up should occur already in low-mass stars (with $M_{\rm i} \gtrsim 1.2$–$1.4\,{\rm M}_\odot$) and be, on average, more efficient ($\lambda \approx 0.5$–0.6), than usually predicted by most full AGB calculations.

Figure 11 shows the best fits to the observed CSLFs in the Large and Small Magellanic Clouds, as obtained from [68], to which the reader is referred for more details. According to that analysis, the most remarkable differences between the two observed distributions (i.e., peak location and shape of the tails) are mainly the expression of different initial metallicities, characterizing the stellar populations in the two host galaxies (i.e., on average, $Z = 0.008$ for the LMC, and $Z = 0.004$ for the SMC).

In particular, the metallicity-dependence of the third dredge-up is found to play the dominant role. At decreasing metallicity the minimum mass, $M_{\rm min}^{\rm carb}$, for a star to experience convective dredge-up of carbon decreases (i.e., $\approx 1.3\,{\rm M}_\odot$ for the LMC, and $\approx 1.2\,{\rm M}_\odot$ for the SMC), and the efficiency of the third dredge-up increases (i.e., on average, $\lambda \approx 0.55$ for the LMC, and $\lambda \approx 0.65$ for the SMC). Moreover, for a given stellar mass the onset of the

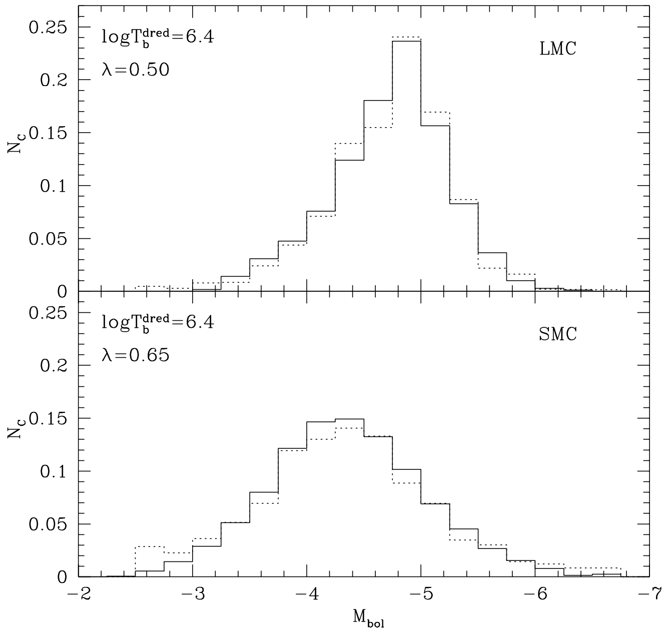

Fig. 11. Observed CSLFs (dotted lines) in the LMC ([19], top panel) and SMC ([81], bottom panel), and the theoretical best fits (solid lines, [68]). The first bin of the observed CSLF in the SMC contains all stars fainter than $M_{\rm bol} = -2.5$. The quantity $T_{\rm b}^{\rm dred}$, a parameter related to $M_{\rm c}^{\rm min}$, represents the minimum temperature at the base of the convective envelope for the occurrence of the third dredge-up, as derived from stellar envelope integrations.

third dredge-up is expected to be favored at lower metallicity, i.e., the lower Z is, the lower $M_{\rm c}^{\rm min}$ is (see Figure 4). In general, both distributions would involve stellar progenitors with initial masses in the range from $M_{\rm min}^{\rm carb}$ up to about 4.5–5.0 $\mathrm{M}_{\odot}$, corresponding to ages from a few 10^9 down to about 10^8 yr.

6.2.1 The Low-Luminosity Tail

The faint tail of observed CSLFs deserves some important remarks. First of all, synthetic AGB models (cf. [32, 49, 66, 68]) have clearly shown that the well-extended and long-lived low-luminosity dip in the light curve of lower-mass AGB stars (cf. Section 3.4.3) has an important effect in shaping the tail of the CSLFs towards fainter luminosities. Just recall, for instance, that a low-mass AGB star can spend as much as ≈ 20–30% of an interpulse period at a luminosity quite lower than expected by the $M_{\rm c}$-L relation. Moreover, we should consider that the initial stages of the TP-AGB evolution occur at lower luminosities, and with a steeper rate of luminosity increase, than predicted by the M_c-L relation for the same core mass (see Section 3.4.2).

Another factor that may affect the low-luminosity extension of the CSLF is the contamination by faint carbon stars formed in closed binary systems, in which the surface of a low-mass star has been contaminated by the ejecta of a former AGB star companion (e.g., [25], Chapter **??**). It was shown by [113] that the CSLF in the SMC is characterized by an extended tail down to $M_{\rm bol} \approx -1.8$. These carbon stars (e.g., J-type stars, dwarf carbon stars, R stars) are indeed too faint to be explained as the result of single-star evolution. However, it should be noted that in the case of the SMC the fraction of the faintest carbon stars amounts to less than 3 % of the total sample [81], so that the calibration procedure applied by [68] should not be affected.

6.2.2 The High-Luminosity Tail

The luminosity distribution of carbon stars in the brightest bins is mainly affected by two factors: mass loss and hot bottom burning. The former controls the luminosity excursion of the most massive carbon stars (since it determines the end of the AGB as soon as the residual stellar envelope is ejected); the latter prevents the most massive and luminous AGB stars from becoming carbon stars.

Unfortunately, the efficiency of both processes is still affected by large uncertainties. However, important indications can be indirectly derived from other observables, e.g., the initial–final mass relation (related to mass loss; cf. Section 6.1), the maximum luminosities of observed AGB stars (related to the overluminosity produced by HBB; see Section 3.4.4), the chemical composition of most luminous AGB stars (related to the efficiency of HBB; see Section 3.8.3).

6.2.3 Number Ratios $N_{\rm C}/N_{\rm M}$

As for the carbon stars, an important additional constraint to the models would be a luminosity function of the M-type AGB stars. However, no reliable LF exists, since most investigators have focused on carbon stars. A constraint that is available is the observed number ratio of carbon to M-type stars ($N_{\rm C}/N_{\rm M}$). One source of uncertainty is that not all M-type stars should be on the TP-AGB. Such uncertainty is reflected in the fact that the $N_{\rm C}/N_{\rm M}$ ratio strongly depends on the spectral type that is included. For the LMC, [5] gives $N_{\rm C}/N_{\rm M2+} = 0.2 \pm 0.1$, $N_{\rm C}/N_{\rm M5+} = 0.80 \pm 0.03$, and $N_{\rm C}/N_{\rm M6+} = 2.2 \pm 0.1$, respectively. It seems plausible to assume that M-stars with spectral type later than M5 are on the TP-AGB. The $N_{\rm C}/N_{\rm M}$ ratio in Local Group galaxies is discussed in [39].

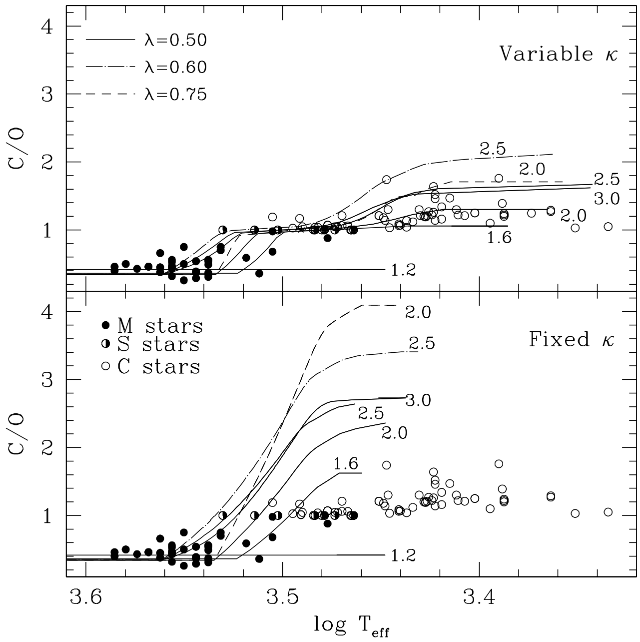

Fig. 12. Effective temperatures as a function of the C/O ratio in Galactic giants. Observed data for Galactic M, S, and C stars (circles) are compared to predictions of synthetic TP-AGB models (lines; see [65]) of different masses (indicated in $M_{\odot}$ near the corresponding curves), assuming different dredge-up efficiencies λ, and adopting either "chemically fixed" opacities (bottom panel), or "chemically variable" opacities (top panel).

6.3 Effective Temperatures of AGB Stars

Observationally, a notable dichotomy exists in effective temperatures and infrared colors between M-type and carbon stars. Carbon stars are systematically cooler and redder than M-type stars. HR-diagrams in the near infrared (e.g., K vs. $J - K$), provided by extensive surveys like DENIS and 2MASS, have clearly shown that carbon stars deviate from the M-type part of the AGB, populating a plume toward redder colors and lower $T_{\rm eff}$. This feature is closely related to marked differences in molecular opacities pertaining to the atmospheres of AGB stars with different C/O ratio. In summary, the abrupt change in the dominant opacity source as C/O grows from below to above unity, i.e., at the transition from oxygen-rich to carbon-rich configurations, causes a remarkable cooling of the HR TP-AGB tracks for carbon stars. This point, explored by [91] and more recently by [65], is illustrated in Figure 12 for a sample of Galactic giants.

The observed data indicate two major facts: (i) the almost complete segregation in effective temperature between M-type and carbon stars; and (ii) the relatively low C/O values (< 2) measured in carbon stars. A comparison is performed with two sets of TP-AGB synthetic models [65], which differ only in the adopted prescriptions for low-temperature opacities κ (for $\log T < 3.7$). They are assumed to be either fixed for solar-scaled abundances of C and O (hence C/O ≈ 0.48, bottom panel), or variable according to the actual C/O ratio, which controls the molecular concentrations involving C and O atoms (top panel). All models are followed from the first TP to the end of the AGB. The main result is that the models with variable opacities succeed in reproducing the observed range of effective temperatures of carbon stars, while this is not the case for fixed solar-scaled abundance opacities.

6.4 Abundances in Planetary Nebulae

According to a commonly recognized scenario, AGB stars are the direct stellar progenitors of PNe, so that the nebular abundances are expected to be the record of the evolution of the photospheric composition during the stellar lifetimes. It follows that the abundances in PNe can be used to improve our understanding of stellar nucleosynthesis and convective mixing, as well as to constrain the basic model parameters in synthetic AGB evolution (i.e., dredge-up parameters, mass loss law, and initial conditions).

Three distinct groups of PNe progenitors are expected. The first group consists of stars with initial masses too low (e.g., $M_\mathrm{i} < 1.2\,\mathrm{M}_\odot$ for the case of the LMC) to experience the third dredge-up. These PNe should exhibit the same stellar abundances as changed—with respect to the main sequence values—by the occurrence of the first dredge-up and RGB extra-mixing process only. Specifically, a modest increase in He and N abundances is expected. The second group consists of stars with initial masses high enough to experience the third dredge-up but too low for HBB to occur on the TP-AGB (e.g., typically $1.2\,\mathrm{M}_\odot \lesssim M_\mathrm{i} \lesssim 3.5\,\mathrm{M}_\odot$). Prior to this phase, further chemical changes should have occurred via the first dredge-up, and possibly the second dredge-up for the massive stars of this group. An increase in He, C, and N abundances is usually predicted for the resulting PNe. The third group consists of stars massive enough to have HBB on the TP-AGB, in addition to the earlier first and second dredge-up processes (with $M_\mathrm{i} \gtrsim 3.5$–$4.0\,\mathrm{M}_\odot$). A more marked increment of He and N and a decrease of C are expected to characterize the nebular abundances. These theoretical groups should explain the empirical classification based on measured PNe abundances, e.g., type I and II PNe first introduced by [79].

If the lifetime of the PNe phase is t_PN, and since there is essentially no nucleosynthesis in the post-AGB and PNe phase itself, we can make the very approximate assumption that the space-average abundance pattern observed in PNe should represent the time-average abundance pattern of the ejecta in AGB stars over the last t_PN years of AGB evolution.

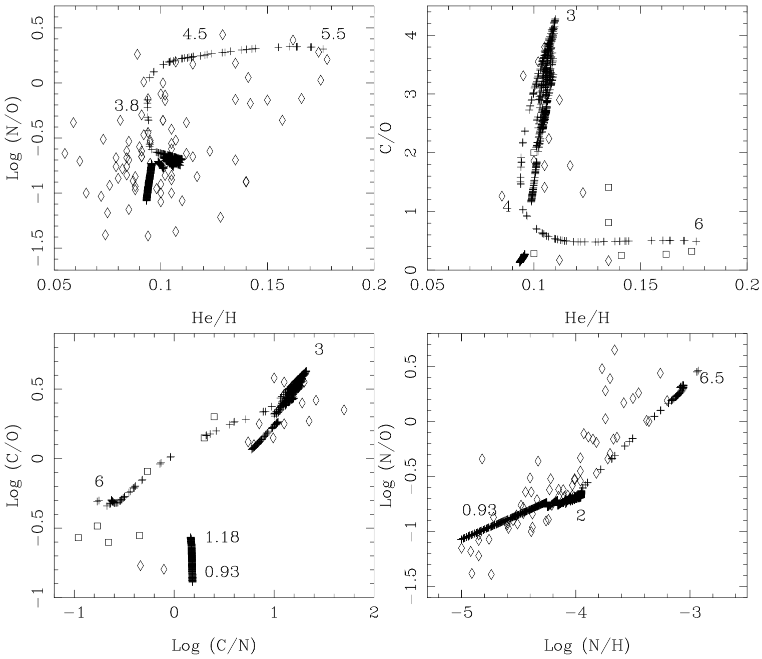

Fig. 13. Observed and predicted abundance ratios of PNe in the LMC. Model predictions (+ signs) and some initial stellar masses are indicated. In the C/O–He/H and C/O–C/N diagram the observed type I PNe (defined as having N/O > 0.5) are indicated by diamonds, the other observed PNe by squares. The density of the theoretical points reflect the IMF and SFR history. From [33].

A complication is that during the running of the synthetic AGB evolution code, based on the Monte Carlo simulation method, one a priori does not know when a star has less than $t_{\rm PN}$ years of AGB evolution left. However, one can make a good estimate of the remaining AGB lifetime by calculating at each time step whether $M_{\rm env}/\dot{M} < t_{\rm PN}$. If so, one can then keep track of the amount of mass lost (the mass in the shell of a PN is another measurable quantity) and the average abundances in the ejecta.

There are a few additional comments to be made. First, not all AGB stars may actually turn into PNe, or be recognized as such. Low-mass stars may produce very low surface-brightness PNe that have not been discovered yet. In fact, the post-AGB and the central star of the PNe may evolve so slowly that the ejecta are dispersed in the interstellar medium before the central star is hot enough to ionize the ejecta. The procedure outlined above merely indicates that *if* a PN is observed, the abundance pattern should be the one calculated in this way. Another complication is from the observational side. The nebulae are strongly shaped by hydrodynamics, and so the abundance patterns, as ejected at the time of AGB evolution, may have been lost when these structures were formed. On average, the abundances should not have changed, but with a spectroscopic observation the slit has to be placed over the nebulae, and this may introduce a bias. The second effect is that gaseous material may condense into grains. This depends on the atom, and so specific elements may be depleted in the gas phase.

This scheme was applied by [33, 38, 66] to the abundances of PNe in the LMC and the Galaxy, respectively. The three groups of stars mentioned above could clearly be identified, and the overall agreement between observations and the synthetic model calculations was satisfactory. An example of these synthetic calculations of PNe abundances is presented in Figure 13, showing a comparison between predictions and observations of PNe in the LMC.

6.5 Pulsating Stars

Historically, variable AGB stars have been divided into three classes: Mira variables, semiregular (or SR) variables, and irregular variables (see Chapters **??** and **??**). The distinction between the classes is in the amplitude of the light variation in the V-band and the periodicity of the light variation.

Since stars are unstable to pulsation only in a small region of the Herzsprung–Russell diagram (the instability strip), and since Miras and SR variables are known to obey period–luminosity relations, variable stars can in principle provide constraints that can aid in an understanding of the evolution of AGB stars in general. Problems are that (i) the location of the instability strip in the $T_{\rm eff}$-$M_{\rm bol}$ plane is not known a priori, (ii) the fact that stars can pulsate in different modes, or possibly even switch modes (e.g., [23, 119]), and (iii) that the so-called pulsation constant that theoretically relates pulsation period to stellar mass and radius is not accurately known.

Despite these difficulties, the only attempt so far to incorporate observations of variable stars in the LMC in synthetic evolution models was by [34]. There, details are given of the recipes used and the observational data available at the time. The conclusion was that long-period variables dominantly pulsate in the fundamental mode.

Since then, in particular, the observational data set has increased dramatically through the micro-lensing projects, MACHO, EROS, OGLE. Most impressively, [119] has used MACHO data to identify five distinct sequences of variable stars in the LMC that show that Miras pulsate in the fundamental mode, and SRs predominantly pulsate in the first, second or third overtone; see Chapter **??**. Two of the five sequences identified do not correspond to single AGB star evolution. Similar work using EROS data has been done by [18].

6.6 Synthetic Colors

An additional constraint that can be used is the colors of stars. For a star with a certain luminosity, effective temperature, and mass-loss rate, at a certain distance, one can calculate the spectral energy distribution using a stellar atmosphere model and a dust radiative transfer program, and calculate the colors in the different photometric bands. To incorporate this in a synthetic evolution program would be very time-consuming; attempts have been made, however (e.g., [58]). A semianalytical approach was adopted by [32] and presented in their Appendix A. The specific question addressed there was whether the observed luminosity function of AGB stars in the LMC is biased because the stars with high mass-loss rates are so red and faint in the optical that they would have escaped detection using classical search methods. Alternatively, the approach was used to estimate which fraction of stars escaped detection with the IRAS satellite, which operated at 12 and 25 μm at the detection limit of the expected fluxes for mass-losing AGB stars. This aspect of obscured AGB stars in the Magellanic Clouds has gained considerable attention recently, both from the analysis of individual objects [97], and searches for, and studies of, a sample of objects using the ISO satellite (e.g., [31, 96, 104]). A major step forward will be provided by the 2MASS and DENIS near-infrared surveys ([3, 22]), which will detect virtually the entire AGB population in the direction of the Magellanic Clouds ([17, 102]).

One of the most surprising results of the IRAS satellite mission was the discovery of carbon stars with 60 μm excess emission [114]. It was shown by [121] that also some M- and S-stars show such an excess. The conclusion was that there must be a shell of very cold dust surrounding the star. Later on, this picture was confirmed with the detection of a thin shell of CO around some of these stars ([62, 73, 74, 75]) and more detailed studies of the extended dust emission ([40, 51, 52]). The interpretation is that there was a brief phase of very high mass loss. After this phase, mass loss dropped, and the shell coasted outward. Recently, mass loss has resumed, as evidenced by the detection of CO close to the central star in some cases. This modulation of the mass loss, and the time scales involved, suggest a possible link with a modulation of the mass loss related to the change in luminosity over a TPC. Early attempts to determine the mass-loss rates in the various phases of the modulation, and to calculate the changes of the IRAS fluxes at 12, 25, and 60 μm as a function of time, are given by [15, 36, 115]. More recent studies that use the luminosity variations of full stellar evolutionary models, coupled to hydrodynamical calculations of the stellar wind, are given by [93]. They suggest that the observed thin shells are the result of interaction of winds with different velocity and density. Note, however, that for the less-studied objects with a 60 μm excess the alternative interpretation that this is simply due to Galactic cirrus cannot be excluded.

7 Conclusions and Outlook

This chapter describes the basic ingredients of a synthetic AGB evolution model. The advantages over full stellar evolutionary models are the computational speed and the fact that the dependence of parameters like the mass-loss law or dredge-up efficiency can be easily changed, and their influence on observable quantities investigated. In fact, by using synthetic models to constrain these parameters, important feedback can be given to the stellar evolution community.

The largest uncertainties for both the full and synthetic evolutionary models refer to the description of the mass loss and the third dredge-up process. Both are crucial in understanding the detailed evolution on the AGB and the formation of S-type and carbon stars. Advances can be made on several levels. First, by detailed modeling of the properties of individual stars. For example, it will be computationally possible in the near future to combine the output of a stellar evolution model $[L(t), T_{\rm eff}(t), \dot{M}(t)]$ with a hydrodynamical model (see Chapter **??**) to make detailed predictions of the density structure around specific stars for specific mass-loss laws, and compare these to the density structure derived from interferometric observations.

Up to now, synthetic models have been used to fit data in our Galaxy, SMC, and LMC only. High-quality data on AGB populations in other galaxies have become available as well as information on the overall SFRs in these galaxies from detailed modeling of color–magnitude diagrams from HST observations (see Chapter **??**). Since these galaxies cover a range of metallicity and SFR histories, fitting the luminosity function and other properties of C- and M-stars in these galaxies might give additional information on mass-loss laws and dredge-up efficiencies.

Finally, a new perspective on the role of pulsation in AGB evolution has been brought up by the microlensing surveys, as detailed in Section 6.5. That pulsation and mass loss are connected is beyond doubt, but a fully self-consistent picture is missing. Questions are whether AGB stars are pulsationally unstable during their entire evolution, and whether mode changes occur, possibly related to the phase in the thermal pulse cycle. The large number of red giant variable stars discovered in the MCs may allow these questions to be addressed in a statistical way.

Acknowledgments

P.M. thanks Léo Girardi for helpful advice during the preparation of the manuscript.

References

1. Arndt, T. U., Fleischer, A. J., and Sedlmayr, E. *A&A*, 327, 614, 1997.
2. Bedijn, P. J. *A&A*, 205, 105, 1988.
3. Beichman, C. A., Chester, T. J., Cutri, R., et al. *PASP*, 110, 367, 1998.
4. Bessell, M. S., Brett, J. M., Scholz, M., et al. In Nomoto, K., editor, *IAU Colloq. 108: Atmospheric Diagnostics of Stellar Evolution*, page 187. Springer-Verlag, Berlin, New York, 1988.

5. Blanco, V. M. and McCarthy, M. F. *AJ*, 88, 1442, 1983.
6. Blöcker, T. and Schönberner, D. *A&A*, 244, L43, 1991.
7. Bloecker, T. *A&A*, 297, 727, 1995.
8. Boothroyd, A. I. and Sackann, I. J. *ApJ*, 328, 632, 1988.
9. Boothroyd, A. I. and Sackmann, I. J. *ApJ*, 328, 641, 1988.
10. Boothroyd, A. I. and Sackmann, I. J. *ApJ*, 328, 653, 1988.
11. Boothroyd, A. I. and Sackmann, I. J. *ApJ*, 328, 671, 1988.
12. Boothroyd, A. I. and Sackmann, I. J. *ApJL*, 393, L21, 1992.
13. Bowen, G. H. *ApJ*, 329, 299, 1988.
14. Bryan, G. L., Volk, K., and Kwok, S. *ApJ*, 365, 301, 1990.
15. Chan, S. J. and Kwok, S. *J. R. Astron. Soc. Can.*, 82, 287, 1988.
16. Chiappini, C., Matteucci, F., and Gratton, R. *ApJ*, 477, 765, 1997.
17. Cioni, M. R., Loup, C., Habing, H. J., et al. *A&AS*, 144, 235, 2000.
18. Cioni, M.-R., Marquette, J.-B., Loup, C., et al. *A&A*, 377, 945, 2001.
19. Costa, E. and Frogel, J. A. *AJ*, 112, 2607, 1996.
20. D'Antona, F. and Mazzitelli, I. *ApJ*, 470, 1093, 1996.
21. Dominguez, I., Chieffi, A., Limongi, M., and Straniero, O. *ApJ*, 524, 226, 1999.
22. Epchtein, N., Deul, E., Derriere, S., and et al. *A&A*, 349, 236, 1999.
23. Feast, M. In Le Bertre, T., Lébre, A., and Waelkens, C., editors, *IAU Symp. 191: Asymptotic Giant Branch Stars*, page 109. ASP, San Francisco, 1999.
24. Fleischer, A. J., Gauger, A., and Sedlmayr, E. *A&A*, 266, 321, 1992.
25. Frantsman, J. *A&A*, 319, 511, 1997.
26. Frost, C. A., Cannon, R. C., Lattanzio, J. C., Wood, P. R., and Forestini, M. *A&A*, 332, L17, 1998.
27. Frost, C. A. and Lattanzio, J. C. *ApJ*, 473, 383, 1996.
28. Gingold, R. A. *ApJ*, 193, 177, 1974.
29. Girardi, L. and Bertelli, G. *MNRAS*, 300, 533, 1998.
30. Girardi, L., Bressan, A., Bertelli, G., and Chiosi, C. *A&AS*, 141, 371, 2000.
31. Groenewegen, M. A. T. and Blommaert, J. A. D. L. *A&A*, 332, 25, 1998.
32. Groenewegen, M. A. T. and de Jong, T. *A&A*, 267, 410, 1993.
33. Groenewegen, M. A. T. and de Jong, T. *A&A*, 282, 127, 1994.
34. Groenewegen, M. A. T. and de Jong, T. *A&A*, 288, 782, 1994.
35. Groenewegen, M. A. T. and de Jong, T. *A&A*, 283, 463, 1994.
36. Groenewegen, M. A. T. and de Jong, T. *A&A*, 282, 115, 1994.
37. Groenewegen, M. A. T., Smith, C. H., Wood, P. R., Omont, A., and Fujiyoshi, T. *ApJL*, 449, L119, 1995.
38. Groenewegen, M. A. T., van den Hoek, L. B., and de Jong, T. *A&A*, 293, 381, 1995.
39. Groenewegen, M. In Le Bertre, T., Lébre, A., and Waelkens, C., editors, *IAU Symp. 191: Asymptotic Giant Branch Stars*, page 535. ASP, San Francisco, 1999.
40. Hashimoto, O., Izumiura, H., Kester, D. J. M., and Bontekoe, T. R. *A&A*, 329, 213, 1998.
41. Havazelet, D. and Barkat, Z. *ApJ*, 233, 589, 1979.
42. Herwig, F. In Noels, A., Fraiponi-Caro, D., Gabriel, M., Grevesse, N., and Demarque, P., editors, *32nd Liège Int. Astrophys. Coll.: Stellar Evolution: What should be done*, page 441. Institut d'astrophysique de Liège, 1997.
43. Herwig, F. *A&A*, 360, 952, 2000.

44. Herwig, F., Blöcker, T., Schönberner, D., and El Eid, M. In Truran, J. and Nomoto, K., editors, *IAU Symp. 187: Cosmic Chemical Evolution*, page 42. International Astronomical Union, 1997.
45. Holtzman, J. A., Gallagher, J. S., Cole, A. A., and et al. *AJ*, 118, 2262, 1999.
46. Iben, I. *ApJ*, 217, 788, 1977.
47. Iben, I. *ApJ*, 246, 278, 1981.
48. Iben, I. and Laughlin, G. *ApJ*, 341, 312, 1989.
49. Iben, I. and Renzini, A. *ARA&A*, 21, 271, 1983.
50. Iben, I. and Truran, J. W. *ApJ*, 220, 980, 1978.
51. Izumiura, H., Hashimoto, O., Kawara, K., Yamamura, I., and Waters, L. B. F. M. *A&A*, 315, L221, 1996.
52. Izumiura, H., Waters, L. B. F. M., de Jong, T., et al. *A&A*, 323, 449, 1997.
53. Jeffries, R. D. *MNRAS*, 288, 585, 1997.
54. Kippenhahn, R. *A&A*, 102, 293, 1981.
55. Knapp, G. R. and Morris, M. *ApJ*, 292, 640, 1985.
56. Koester, D. and Reimers, D. *A&A*, 313, 810, 1996.
57. Kudritzki, R. P., Pauldrach, A., and Puls, J. *A&A*, 173, 293, 1987.
58. Lançon, A. In Le Bertre, T., Lébre, A., and Waelkens, C., editors, *IAU Symp. 191: Asymptotic Giant Branch Stars*, page 579. ASP, San Francisco, 1999.
59. Lattanzio, J. C. *ApJ*, 311, 708, 1986.
60. Lattanzio, J. C. *ApJL*, 344, L25, 1989.
61. Lattanzio, J. C. *Proceedings of the Astronomical Society of Australia*, 10, 120, 1992.
62. Lindqvist, M., Olofsson, H., Lucas, R., et al. *A&A*, 351, L1, 1999.
63. Marigo, P. *A&A*, 340, 463, 1998.
64. Marigo, P. *A&A*, 370, 194, 2001.
65. Marigo, P. *A&A*, 387, 507, 2002.
66. Marigo, P., Bressan, A., and Chiosi, C. *A&A*, 313, 545, 1996.
67. Marigo, P., Bressan, A., and Chiosi, C. *A&A*, 331, 564, 1998.
68. Marigo, P., Girardi, L., and Bressan, A. *A&A*, 344, 123, 1999.
69. Marigo, P., Girardi, L., and Chiosi, C. *A&A*, 316, L1, 1996.
70. Marigo, P., Girardi, L., Weiss, A., and Groenewegen, M. *A&A*, 351, 161, 1999.
71. Matteucci, F. *Fundamentals of Cosmic Physics*, 17, 283, 1996.
72. Mowlavi, N. *A&A*, 344, 617, 1999.
73. Olofsson, H., Bergman, P., Eriksson, K., and Gustafsson, B. *A&A*, 311, 587, 1996.
74. Olofsson, H., Bergman, P., Lucas, R., et al. *A&A*, 353, 583, 2000.
75. Olofsson, H., Carlstrom, U., Eriksson, K., Gustafsson, B., and Willson, L. A. *A&A*, 230, L13, 1990.
76. Paczynski, B. *Acta Astronomica*, 20, 47, 1970.
77. Paczynski, B. *ApJ*, 202, 558, 1975.
78. Pagel, B. E. J. and Tautvaisiene, G. *MNRAS*, 299, 535, 1998.
79. Peimbert, M. In Terzian, Y., editor, *IAU Symp. 76: Planetary Nebulae*, page 215. D. Reidel Publishing Co., Dordrecht, 1978.
80. Pols, O. R., Schroder, K.-P., Hurley, J. R., Tout, C. A., and Eggleton, P. P. *MNRAS*, 298, 525, 1998.
81. Rebeirot, E., Azzopardi, M., and Westerlund, B. E. *A&AS*, 97, 603, 1993.
82. Refsdal, S. and Weigert, A. *A&A*, 6, 426, 1970.
83. Reid, I. N. *AJ*, 111, 2000, 1996.

84. Reimers, D. *Memoires of the Sociètè Royale des Sciences de Liège*, 8, 369, 1975.
85. Renzini, A. and Buzzoni, A. In Chiosi, C. and Renzini, A., editors, *Spectral Evolution of Galaxies*, page 195. D. Reidel Publishing Co., Dordrecht, 1986.
86. Renzini, A. and Fusi Pecci, F. *ARA&A*, 26, 199, 1988.
87. Renzini, A. and Voli, M. *A&A*, 94, 175, 1981.
88. Rocha-Pinto, H. J., Maciel, W. J., Scalo, J., and Flynn, C. *A&A*, 358, 850, 2000.
89. Rocha-Pinto, H. J., Scalo, J., Maciel, W. J., and Flynn, C. *A&A*, 358, 869, 2000.
90. Scalo, J. M., Despain, K. H., and Ulrich, R. K. *ApJ*, 196, 805, 1975.
91. Scalo, J. M. and Ulrich, R. K. *ApJ*, 200, 682, 1975.
92. Schaller, G., Schaerer, D., Meynet, G., and Maeder, A. *A&AS*, 96, 269, 1992.
93. Steffen, M., Szczerba, R., and Schoenberner, D. *A&A*, 337, 149, 1998.
94. Straniero, O., Chieffi, A., Limongi, M., et al. *ApJ*, 478, 332, 1997.
95. Tinsley, B. M. *Fundamentals of Cosmic Physics*, 5, 287, 1980.
96. Trams, N. R., van Loon, J. T., Waters, L., and et al. *A&A*, 346, 843, 1999.
97. Trams, N. R., van Loon, J. T., Zijlstra, A. A., and et al. *A&A*, 344, L17, 1999.
98. Travaglio, C., Galli, D., Gallino, R., et al. *ApJ*, 521, 691, 1999.
99. Tuchman, Y., Glasner, A., and Barkat, Z. *ApJ*, 268, 356, 1983.
100. van den Hoek, L. B. PhD thesis, Univ. of Amsterdam, 1997.
101. van den Hoek, L. B. and Groenewegen, M. A. T. *A&AS*, 123, 305, 1997.
102. van Dyk, S. D., Cutri, R. M., Skrutskie, M. F., and Egan, M. In *American Astronomical Society Meeting*, volume 193, page O809. American Astronomical Society, 1998.
103. van Loon, J. T. *A&A*, 354, 125, 2000.
104. van Loon, J. T., Groenewegen, M. A. T., de Koter, A., and et al. *A&A*, 351, 559, 1999.
105. van Loon, J. T., Zijlstra, A. A., Whitelock, P. A., and et al. *A&A*, 329, 169, 1998.
106. Vassiliadis, E. and Wood, P. R. *ApJ*, 413, 641, 1993.
107. Wagenhuber, J. PhD thesis, Techn. Univ. München, 1996.
108. Wagenhuber, J. and Groenewegen, M. A. T. *A&A*, 340, 183, 1998.
109. Weidemann, V. *A&A*, 188, 74, 1987.
110. Weidemann, V. In Rood, R. T. and Renzini, A., editors, *Advances in Stellar Evolution*, page 169. Cambridge University Press, Cambridge, 1997.
111. Weidemann, V. *A&A*, 363, 647, 2000.
112. Weidemann, V. and Koester, D. *A&A*, 121, 77, 1983.
113. Westerlund, B. E., Azzopardi, M., Breysacher, J., and Rebeirot, E. *A&A*, 303, 107, 1995.
114. Willems, F. J. and de Jong, T. *ApJL*, 309, L39, 1986.
115. Willems, F. J. and de Jong, T. *A&A*, 196, 173, 1988.
116. Wood, M. A. *ApJ*, 386, 539, 1992.
117. Wood, P. R. In Iben, I., J. and Renzini, A., editors, *Physical Processes in Red Giants*, page 135. D. Reidel publishing Co., Dordrecht, 1981.
118. Wood, P. R. In Cacciari, C. and Clementini, G., editors, *ASP Conf. Ser. 11: Confrontation Between Stellar Pulsation and Evolution*, page 355. ASP, San Francisco, 1990.

119. Wood, P. R., Alcock, C., Allsman, R. A., and et al. In Le Bertre, T., Lébre, A., and Waelkens, C., editors, *IAU Symp. 191: Asymptotic Giant Branch Stars*, page 151. ASP, San Francisco, 1999.
120. Wood, P. R. and Zarro, D. M. *ApJ*, 247, 247, 1981.
121. Zijlstra, A. A., Loup, C., Waters, L. B. F. M., and de Jong, T. *A&A*, 265, L5, 1992.